

The University of Maine

DigitalCommons@UMaine

---

Electronic Theses and Dissertations

Fogler Library

---

Summer 8-18-2023

# The Performance Analysis and Optimization of Wave Energy Converters From Modeling to Basin Testing

Lauren Dickson

University of Maine, lauren.dickson@maine.edu

Follow this and additional works at: <https://digitalcommons.library.umaine.edu/etd>



Part of the [Ocean Engineering Commons](#)

---

## Recommended Citation

Dickson, Lauren, "The Performance Analysis and Optimization of Wave Energy Converters From Modeling to Basin Testing" (2023). *Electronic Theses and Dissertations*. 3869.

<https://digitalcommons.library.umaine.edu/etd/3869>

This Open-Access Thesis is brought to you for free and open access by DigitalCommons@UMaine. It has been accepted for inclusion in Electronic Theses and Dissertations by an authorized administrator of DigitalCommons@UMaine. For more information, please contact [um.library.technical.services@maine.edu](mailto:um.library.technical.services@maine.edu).

**THE PERFORMANCE ANALYSIS AND OPTIMIZATION  
OF WAVE ENERGY CONVERTERS FROM  
MODELING TO BASIN TESTING**

By

Lauren Dickson

B.S. University of Maine 2021

A THESIS

Submitted in Partial Fulfilment of the

Requirements of the Degree of

Master of Science

(Mechanical Engineering)

The Graduate School

The University of Maine

August 2023

Advisory Committee:

Dr. Richard W. Kimball, Presidential Professor in Ocean Engineering and Energy, Co-Advisor

Dr. Lauren Ross, Associate Professor of Civil Engineering, Co-Advisor

Dr. Andrew Goupee, Donald A. Grant Associate Professor of Mechanical Engineering

© 2023 Lauren Dickson

All Rights Reserved

**THE PERFORMANCE ANALYSIS AND OPTIMIZATION  
OF WAVE ENERGY CONVERTERS FROM  
MODELING TO BASIN TESTING**

By Lauren Dickson

Thesis Advisors: Dr Richard W. Kimball, Dr. Lauren Ross

An Abstract of the Thesis Presented  
In Partial Fulfillment of the Requirements for the  
Degree of Master of Science  
(Mechanical Engineering)  
August 2023

The successful development and optimization of wave energy converters (WECs) are pivotal to the pursuit of sustainable and renewable energy sources. This thesis explores the elements in a workflow that develops and demonstrates the protocols for the optimization of WECs using a rapid design\build\test procedure. This thesis establishes the characterization of scaled ocean test sites, develops the performance metrics, generates the performance modeling techniques to predict the optimum design geometries which will be produced for final testing, and finally, establishes the basin test plan which will be used to conduct the testing on the optimum design. The findings of this research provide insights into WEC behavior and performance evaluation. By standardizing metrics and honing modeling and testing procedures, this thesis contributes to the wider adoption of wave energy as a viable and sustainable source of power. Harnessing the potential of wave energy through this workflow will help positively shape our energy future.

## **DEDICATION**

This thesis is dedicated to my family, David, Linda, Evan, and Maya Dickson for their endless support in my pursuit of higher education. To my two advisors, Dr. Lauren Ross, and Dr. Richard Kimball, who challenged me to be a better student and made my masters experience wonderful. To my fellow Offshore Engineering graduate students for their friendship and commiseration. To my Singers friends, who gave me friendship to last a lifetime. Lastly, to Sam, for making me a better person every day.

## **ACKNOWLEDGEMENTS**

This material is based upon work supported by the U.S. Department of Energy's Office of Energy Efficiency and Renewable Energy (EERE) under the Water Power Technologies Office Award Number DE-EE0009448.

## TABLE OF CONTENTS

DEDICATION .....	iii
ACKNOWLEDGEMENTS .....	iv
CHAPTER 1: INTRODUCTION .....	1
CHAPTER 2: SCALED OCEAN TEST SITE CHARACTERIZATION .....	3
2.1 Introduction .....	3
2.2 Environmental Data and Analysis .....	5
2.2.1 JONSWAP .....	9
2.2.2 Beaufort Sea Scale .....	10
2.3 Results .....	11
2.4 Implementation of the Method .....	17
2.5 Applications .....	18
2.6 Discussion .....	21
CHAPTER 3: PERFORMANCE AND COST METRIC DEVELOPMENT .....	22
3.1 Introduction .....	22
3.2 Current Industry Used Metrics .....	24
3.3 Justification and Overview of Developed Metrics .....	24
3.3.1 Geometry Optimization for Power Production Metrics .....	25
3.3.2 Geometry Optimization Metrics for Component Force and Moment Reduction .....	30
3.3.3 Additive Manufacturing Metrics .....	33
3.4 Discussion of Metrics .....	34
3.5 Example Calculations .....	35
CHAPTER 4: POTENTIAL FLOW AND DYNAMIC MODEL WORKFLOW FOR MODEL VALIDATION .....	37
4.1 Introduction .....	37
4.2 Potential Flow Model .....	40
4.2.1 Added Mass and Damping Coefficients .....	41
4.2.2 Excitation Forces .....	42
4.2.3 NEMOH Workflow .....	42
4.2.4 NEMOH to WAMIT .....	45
4.3 Frequency Domain Model .....	48
4.3.1 Frequency Domain Outputs .....	50
4.4 Time Domain Model .....	53
4.5 Discussion of Modeling Discussion .....	54

CHAPTER 5: TEST PLAN DEVELOPMENT FOR WECS.....	58
5.1 Overview .....	58
5.2 Testing Facility Description .....	58
5.3 Froude Scaling Laws .....	60
5.4 Device Description .....	61
5.5 Data Acquisition .....	63
5.6 Test Matrix and Test Conditions .....	64
CHAPTER 6: CONCLUSIONS.....	66
6.1 Future Work.....	67
APPENDICES .....	73
APPENDIX A.....	73
APPENDIX B.....	75
BIOGRAPHY OF AUTHOR.....	78



## CHAPTER 1

### Introduction

To meet the targets set by the International Panel on Climate Change to reduce greenhouse gas emissions, the world will need to gain significant momentum in developing more renewable energy sources [1]. Wave energy, which harnesses the power of ocean waves to generate electricity, has become a promising resource for renewable energy. The global annual potential of different ocean energy sources is significantly greater than our global demand. However, harnessing all the potential energy available from ocean waves is not currently possible on a large scale because most of the ocean energy technologies are still under development [2]. The successful deployment and optimization of wave energy converters (WECs) require a comprehensive understanding of the wave climate at potential test and deployment sites. To facilitate the development of WECs, it is essential to accurately represent the performance of a WEC system's behavior. Model validation and basin testing play crucial roles in this process. To conduct reliable tests and validate numerical models effectively, a representative scaled ocean test site is required, which can be used to inform models and basin test designs. Finally, to evaluate and optimize the WEC models in their environment, performance metrics must be developed. The process of characterizing a scaled ocean test site, developing performance metrics, using dynamic models for validation, and establishing a test plan for basin testing are the focal points of this thesis.

This thesis aims to explore the following points, shown in Figure 1:

- Chapter 2: To perform a comprehensive wave site characterization of a scaled ocean test site and identify a scale ratio to accurately scale devices for testing in such an environment.
- Chapter 3: To develop and establish performance metrics for evaluating the performance of WECs for their desired test goals and enable comparison between different iterations of a device.

- Chapter 4: To accurately model WEC hulls for optimization of energy output by defining a modeling workflow.
- Chapter 5: To develop a basin test plan for reliable model testing.

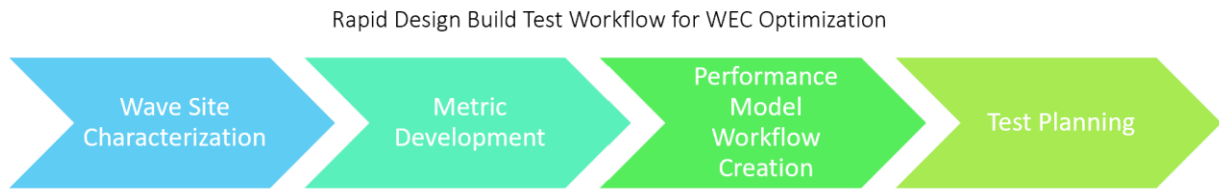


**Figure 1: Flowchart of the rapid design build test workflow for WEC optimization.**

The significance of this study lies in its potential to enhance the understanding of the wave climate within a scaled ocean test environment, and within a controlled test environment, leading to improved accuracy in model validation and basin testing of WECs. Developing and deploying offshore renewable energy technologies comes with several challenges, including the high costs of installation and maintenance, harsh ocean conditions, and potential impacts on marine ecosystems. By characterizing the wave site, engineers will be equipped with valuable information regarding the wave conditions, including wave height period, direction, and spectral content. This knowledge will enable the replication of realistic wave conditions during scale model testing, ensuring reliable and representative results that will help to optimize the device before deploying full-scale models. The scaling methodology presented in this thesis will provide wave environment scaling for any wave site and device size.

The research in each chapter will begin with a literature review pertaining to the topic of the chapter, if applicable. Each chapter is connected through a WEC design optimization workflow. First, a desired test site is characterized; then, metrics are created to ensure fair optimization and comparison between model variants; next, a modeling workflow using potential flow and dynamic models are created for model validation and to ensure output convergence; and last, a basin test plan is created to ensure accurate and methodical testing of the variants. Overall, this thesis aims to contribute to a better understanding of the scale model testing, performance evaluation, dynamic modeling, and basin test plan design of WEC optimization.

## CHAPTER 2

### Scaled Ocean Test Site Characterization

#### 2.1 Introduction

Offshore renewable energy is becoming a popular alternative for non-renewable fossil fuels, and the need for the efficient development of this technology is growing to reduce cost and environmental impact [3]. Early development of renewable energy devices often involves scaled basin testing, which offers a controlled environment for testing, but does not replicate the harsh environmental conditions of the ocean, such as rusting, biofouling, weathering, etc. [4]. An important step in the efficient development of this technology is model validation, which allows developers access to important information about their designs. Model scale testing allows researchers to collect real and accurate data - such as energy production, forces due to waves in extreme conditions, and cost estimates - to validate their full-scale model at the model scale price, and reduces the time and risk involved in full-scale testing [5]. Scaled ocean test sites, such as that of the European Marine Energy Center (EMEC), help to bridge the gap from tank testing to full-scale ocean testing by acting as a step between smaller and larger scale projects [6], which is necessary to gain insight into how the ocean changes the behavior of a device. By offering model data, ocean environment behavior, and a model scale price tag for such information, these scaled ocean test environments can aid in the efficient and informed development of offshore renewable energy devices [7]. In this chapter, a method for the characterization of wave energy resources and a method for identifying a scale ratio for scaled ocean test sites is presented.

Full scale wave farm characterization exists in literature, including at the local and global scale, but little research exists on characterizing a scaled wave farm test site, or identifying its scale ratio. Some wave farm site identification research puts emphasis on power available at a given site [8], or global wave energy resource [9]. Many sites are used for full scale testing, such as the Atlantic Marine Energy Test Site [10] or China's National Ocean Integrated Test Site [11], but there are a few existing scaled ocean test sites, such as EMEC, a Monhegan, Maine test site [12], and a ¼-scale site in Galway Bay in Ireland [13]. When comparing

these full scale test sites for use, many wave statistics such as significant wave height, peak period, wind direction, and wave direction, are often identified, [10], [13], [14], and are used in this chapter to characterize a scaled ocean test site and identify a scale ratio between any two sites of interest [11]. Many developers must characterize their own test sites and identify their scale ratios, and for design validation and optimization in a scaled ocean test site, it is also important to consider proximity of design company to the test site, and how many years of data is available at a given site.

In this chapter, a method for the characterization of wave energy resources in a scaled ocean environment and identifying the environment's scale ratio is outlined using the Castine Scaled Ocean Test Site off the coast of Maine in the Penobscot bay, shown in Figure 2. The case study analyzed for this section is a military controlled test site off the coast of Hawaii, in which a scale ratio will be identified between the Pacific wave environment and the Castine Scaled Ocean Test Site (CSOTS) wave environment. Finally, a scale ratio will be identified between the Pacific site and the University of Maine's Wind Wave laboratory basin using its maximum possible wave height. In following sections, this research is built upon by providing a consistent method for characterizing and identifying the scale ratio of a test site.

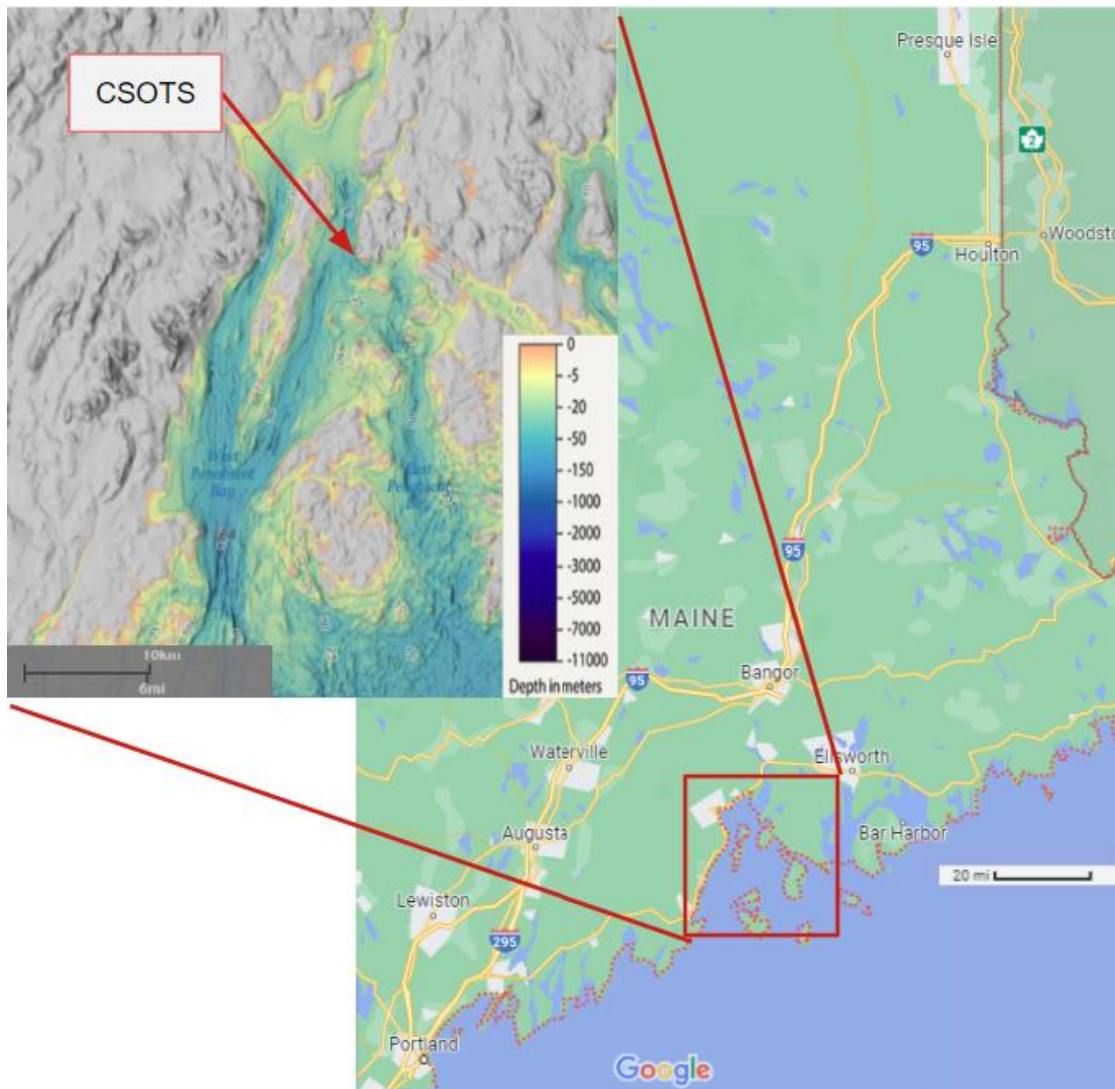


**Figure 2: Location of Castine Scaled Ocean Test Site with Respect to Maine and Penobscot Bay Including Scales and Bathymetry**

## **2.2 Environmental Data and Analysis**

The location chosen for the environmental analysis is Castine Harbor, located off the coast of Castine, Maine, in Penobscot Bay. Penobscot Bay is a semi-sheltered environment because of the six plus islands that protect its inlet, such as Islesboro, North Haven, and Deer Isle. This sheltering, coupled with a relatively high tidal range that allows for much of the bay to exist in transitional to shallow water wave regimes, creating a calm ocean environment off the coast of Castine, which is ideal for a scaled ocean test

site. This environment has previously been used to test model scale projects, such as the VoltturnUS 1:8 [15], which allowed for testing in extreme conditions.

To accurately characterize a scaled ocean test site, data on the wave climate and atmospheric conditions, such as wave height, wave period, wave direction, wind speed, and wind direction, must be collected over a substantial period. Ideally this period would cover multiple years to truly understand the interannual variability of the wave field at the site of interest [13], but only a partial year's worth of data was able to be collected for this project. For CSOTS, wave climate and atmospheric conditions were collected from four SOFAR Spotter wave buoys, shown in the ocean in Figure 3, that were deployed in a cross-shore array shown in Figure 4 from October 2020 to October 2021.

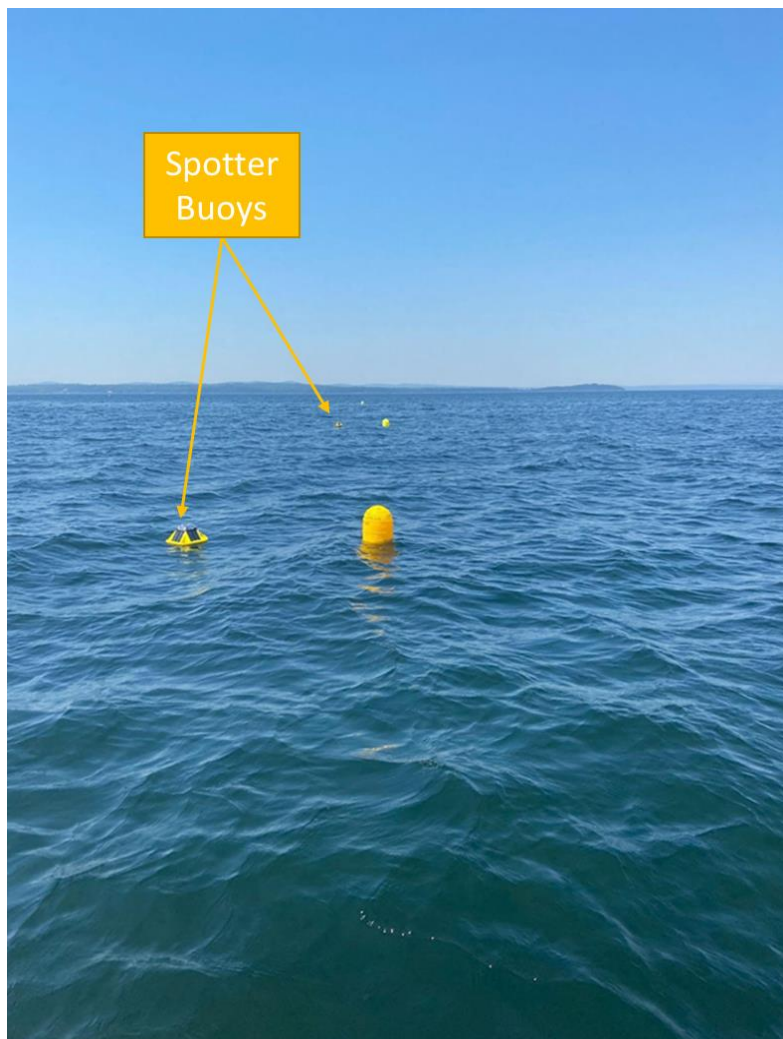


**Figure 3: Spotter Buoys used to collect data in the water at CSOTS**

This cross-shore array (Figure 4) spans intermediate to shallow water wave regimes, where the wave motion spans all the way down the water column to the seabed. Data such as vertical displacement, wind speed, wind temperature, water temperature, and more is transmitted via telemetry from the buoys to the Spotter buoy online platform in 30-minute averaged points. Raw data such as vertical displacements are physically downloaded from their internal memory upon retrieval and is collected at 2.5 Hz, and data such as wavelength can be extracted to identify wave regimes of the buoys. This raw data is used for further post-processing.

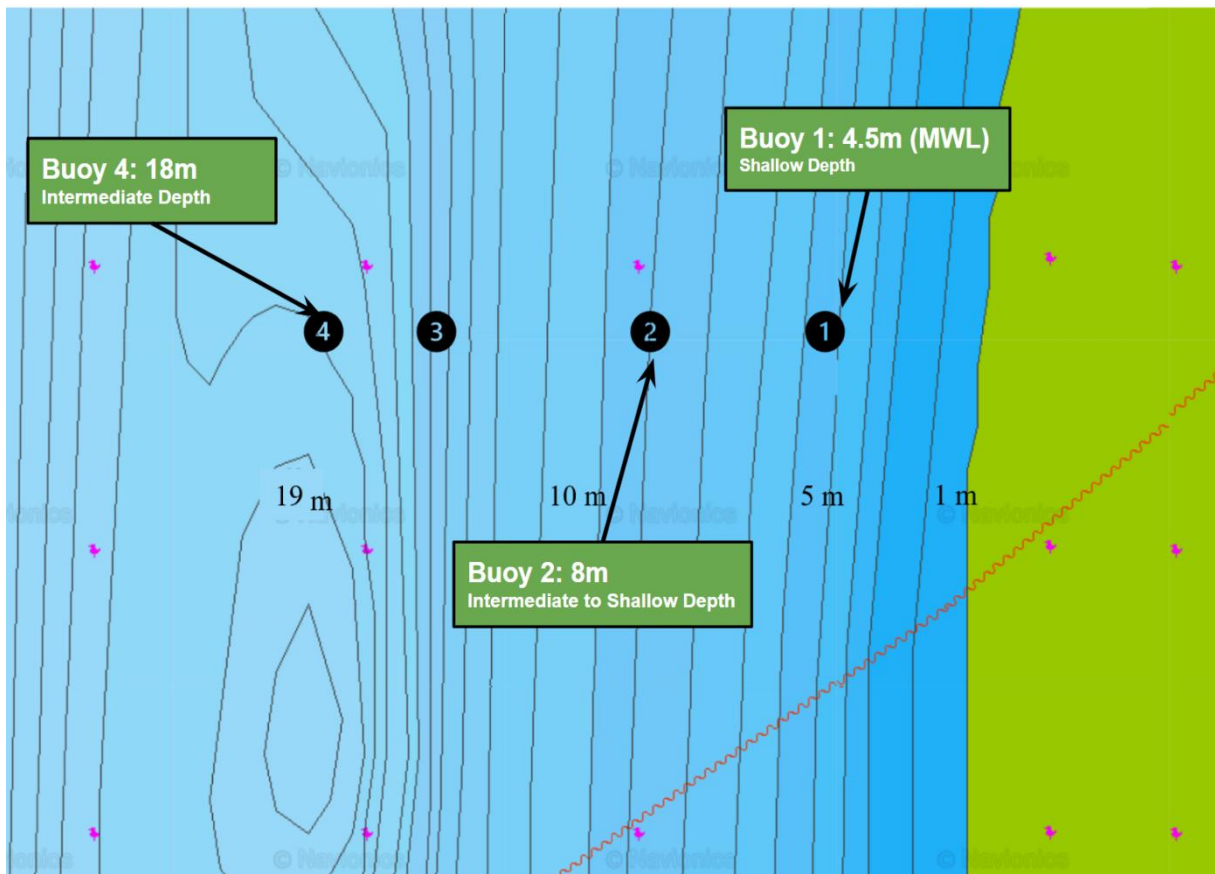


**Figure 4: Cross Shore Array and Bathymetry of Spotter Buoys 1 through 4 in CSOTS including Bathymetry and Depth of Some Buoys. Buoys 1 and 2 cover Shallow to Intermediate Depths while Buoy 4 sits in an Intermediate Depth Range [16]**

Data outliers, such as data (water level variations) below the noise floor of the buoys (0.2 Hz), and wave heights greater than 3 standard deviations away from the mean were removed [17], and the data was

smoothed using averages from every 2 data points. Outliers were removed to eliminate wrongful data that occurs for many reasons, such as when the buoys are picked up out of the water and hauled into a boat for data collection, or when passerby boats create large wakes. A visual of the data parsing shown in Figure 5, where the image on the left shows water level variations from buoy 2 in Winter, and the image on the right shows how the outliers were parsed and the orange data was left.

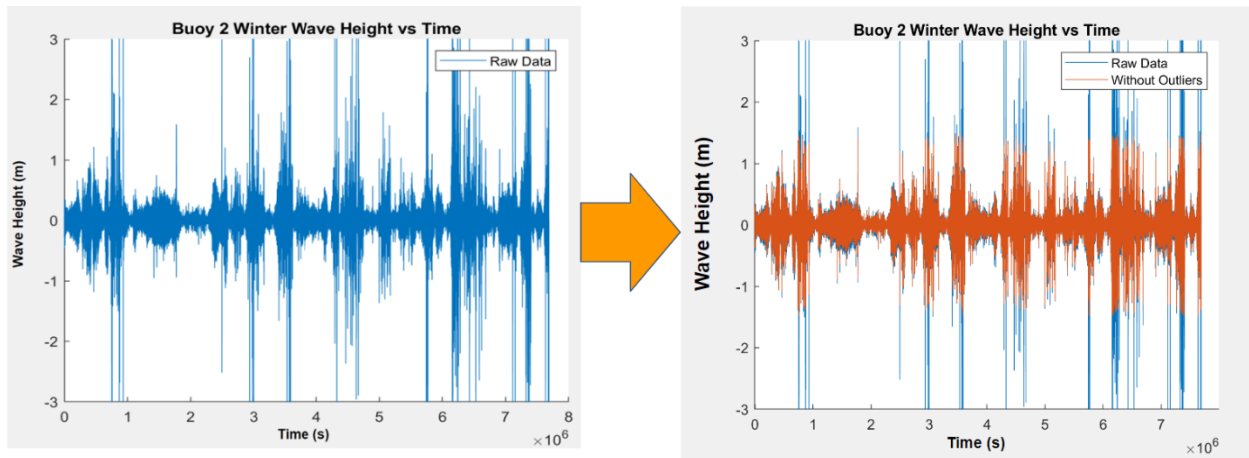


**Figure 5: Raw Water Elevation Data in the CSOTS during the Winter Months that has not been processed on the right**

This processed wave data is put into bins of 30-minute increments, and a JONSWAP spectral analysis using  $\gamma = 1$  to determine the significant wave height and peak period was performed for each bin (JONSWAP in 2.2.1 ). This  $\gamma$  value was chosen because it best represented the spread of the data, which is a well-developed ocean environment. It was also chosen because it best aligns with the Wave Energy Prize (WEP) tests, which is a project that originally used Castine data for WEC testing [18]. This calculation was made using a software package called Oceanlyz [19]. Figure 6 shows how the Power Spectral Density (PSD) of Castine is well represented with a JOHNSWAP where  $\gamma = 1$ .



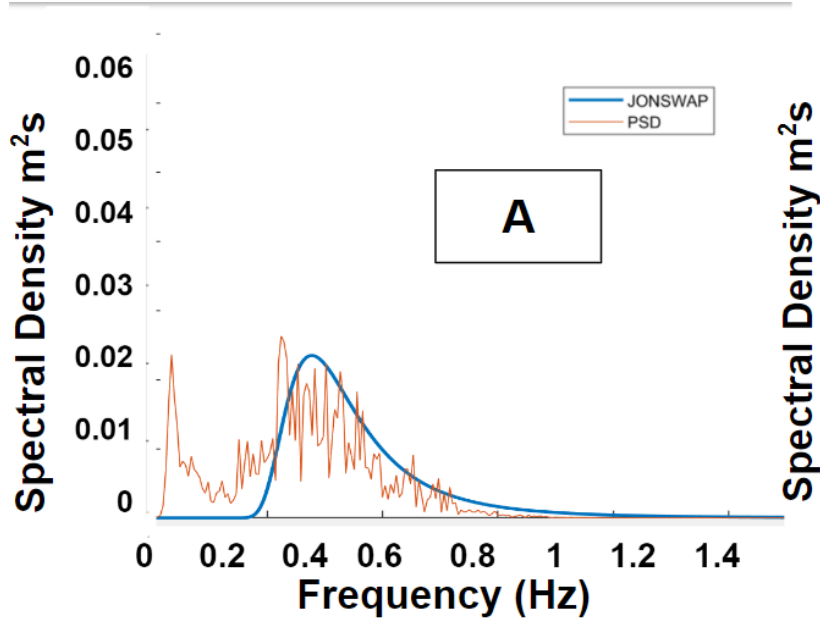


Figure 6: JONSWAP vs PSD of Castine where  $\gamma$  is 1.

### 2.2.1 JONSWAP

The Joint North Sea Wave Project (JONSWAP) [20] spectrum is a tool used to determine the shape of the function governing the energy balance of a wave spectrum. JONSWAP is characterized by spectral parameters of a wave field over a given window that summarize the wave field, such as significant wave height (the average of the top one third of wave heights) and peak period (the wave period related to the significant wave height). These are commonly used parameters that help to characterize a wave environment. The following equations make up the JONSWAP.

$$Sj(f) = (1 - 0.287 \log(\gamma)) \left(\frac{5}{16}\right) Hs^2 \omega_p^4 \omega^{-5} e^{(-1.25 \cdot (\frac{\omega}{\omega_p})^{-4})} \gamma \cdot e^{(-0.5 \cdot (\frac{\omega - \omega_p}{\sigma \omega_p})^2)} \quad (1)$$

$$\omega = 2 \cdot \pi \cdot f \quad (2)$$

$$\omega_p = \frac{2 \cdot \pi}{T_p} \quad (3)$$

Where  $Sj$  is the one-sided wave spectrum in  $m^2/(\text{rad/s})$  and can be converted to  $m^2/\text{Hz}$  by multiplying by  $2\pi$ ,  $\sigma$  is a spectral width parameter (often fixed values  $\sigma_1 = 0.07$ , if frequency is less than peak wave frequency, and  $\sigma_2 = 0.09$  if frequency is greater than or equal to peak wave frequency),  $f$  is the

frequency to compute the spectrum at in Hz,  $H_s$  is the significant wave height in m,  $T_p$  is peak spectral wave period in s, and  $\gamma$  is the peak shape parameter and is unitless.

### **2.2.2 Beaufort Sea Scale**

In 1806, Commander Francis Beaufort created a 13-point scale to give descriptions to wind and sea conditions [21]. Over time, this scale has evolved to include wind speeds and wave heights that are used to understand the state of the ocean on a given day so that mariners today can be prepared for ocean voyages. We use this updated Beaufort scale to explain the conditions of the wave sites we are investigating. Beaufort numbers 0 through 5 and their descriptions are shown in Table 1.

**Table 1: Beaufort Sea State definitions and their descriptions.**

<b>Beaufort Number</b>	<b>Description – Wind</b>	<b>Description – Sea</b>	<b>Wave height (m)</b>
<b>0</b>	Calm.	Sea like a mirror.	0
<b>1</b>	Light air.	Ripples with the appearance of scales, no foam crests.	0 – 0.15
<b>2</b>	Light breeze.	Small, short, wavelets, crests are glassy and do not break.	0.15 – 0.30
<b>3</b>	Gentle breeze.	Large wavelets, crests begin to break, foam forms.	0.30 – 0.90
<b>4</b>	Moderate breeze.	Small waves, becoming longer, more foam.	0.90 – 1.5
<b>5</b>	Fresh Breeze.	Moderate waves, pronounced long form, chance of spray.	1.5 – 2.4
<b>Etc.</b>			

### **2.3 Results**

Wave conditions at CSOTS were sorted into percentage occurrence of Beaufort scale conditions. These occurrences are shown in a histogram chart in Figure 7. This information provides insight into the percentage chance of conditions that the WEC device would endure, in terms of a common scale understood by sea farers. It is clear by the histogram that the prevailing sea states are from state 0 to state 2. Sea states 3-4 occur less than 5 percent of the time. Sea state 5 almost never occurs in this sheltered environment.

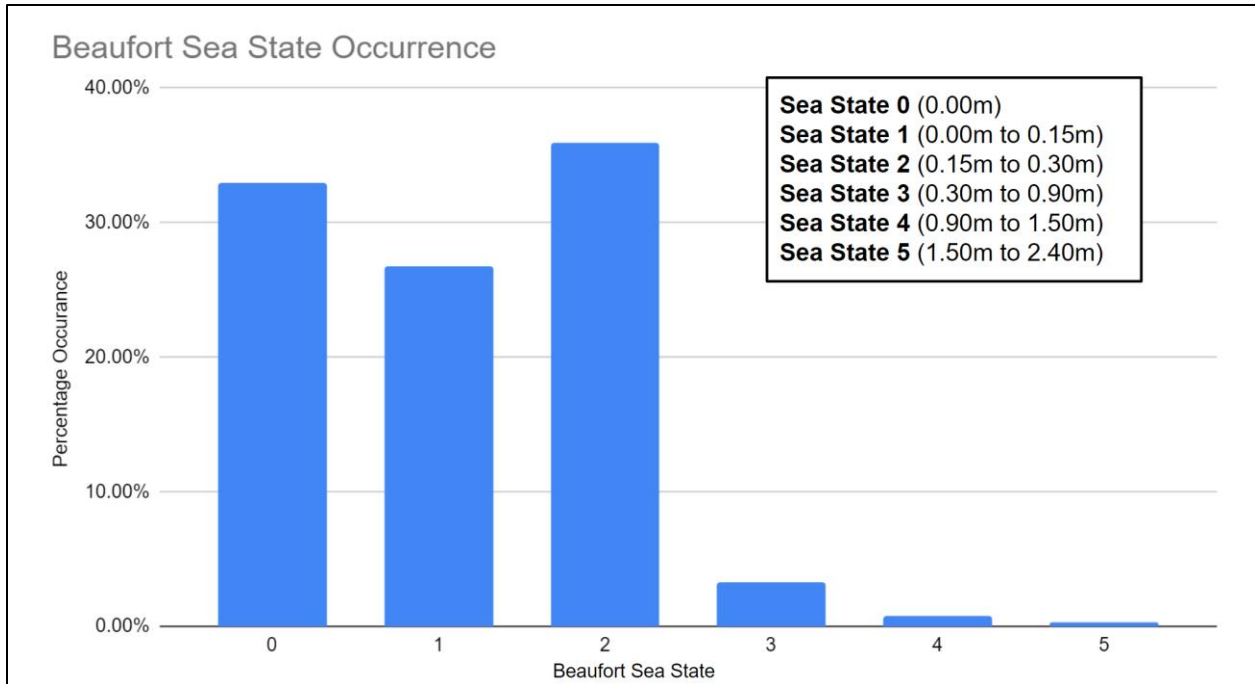


**Figure 7: Histogram of Beaufort Sea State Occurrence in CSOTS with sea state definitions included in top right.**

Wind and wave roses are presented in Figure 8 and show the dominant wind direction and speed (green), and wave direction and height (blue) for a given season. The graphs are arranged into 3 seasons: Fall – A, Winter – B, and Spring – C. Each rose includes rings that represent percentage of occurrence, and are color coordinated to represent wind speeds (green legend on upper right) and wave heights (blue legend on lower right). There are two primary directions for each season between wind and waves: Northwest and Southwest, divided into wave roses in Figure 9 for the entire time span of data. The average wind speed and wave height for the Northwest is 4.48 m/s and 1.01 m, respectively, while the Southwest is 3.34 m/s and 0.99 m, respectively. The Southwest represents the larger percentage of data collected by about 60%, where the activity in the Northwest represents around 40%. Table 2 shows the average wind speed and percentage occurrence divided by season and major direction. Table 3 shows the average wave height and percentage occurrence divided by season and major direction.

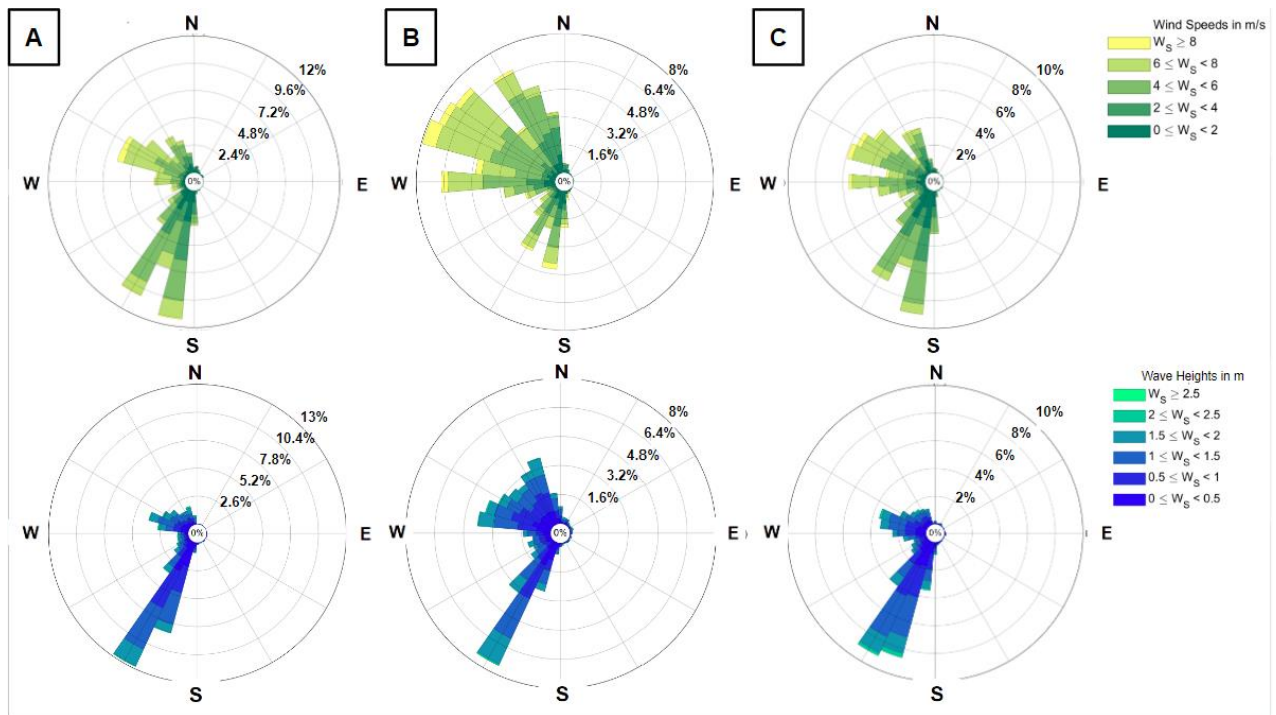


Figure 8: Wind Speed Rose (in Green, on top row) and Wave Height Rose (in blue, on bottom row) for CSOTS for Fall (A), Winter (B), and Spring (C) seasons including their percentage occurrence and legend.

**Table 2: Average Wind Speed and Percent Occurrence by Season and Direction**

Average Wind Speed				
Season	Northwest (m)	% Occur.	Southwest (m)	% Occur.
Fall	4.76	40.97	3.57	59.03
Winter	4.65	60.01	4.12	39.99
Spring	3.51	36.55	2.64	63.45
Average	4.48	42.60	3.34	57.40

**Table 3: Average Wave Height and Percent Occurrence by Season and Direction**

Average Wave Height				
Season	Northwest (m)	% Occur.	Southwest (m)	% Occur.
Fall	1.04	33.51	0.97	66.48
Winter	0.95	55.71	1.03	41.66
Spring	1.04	35.42	0.96	64.58
Average	1.01	37.9	0.99	62.0

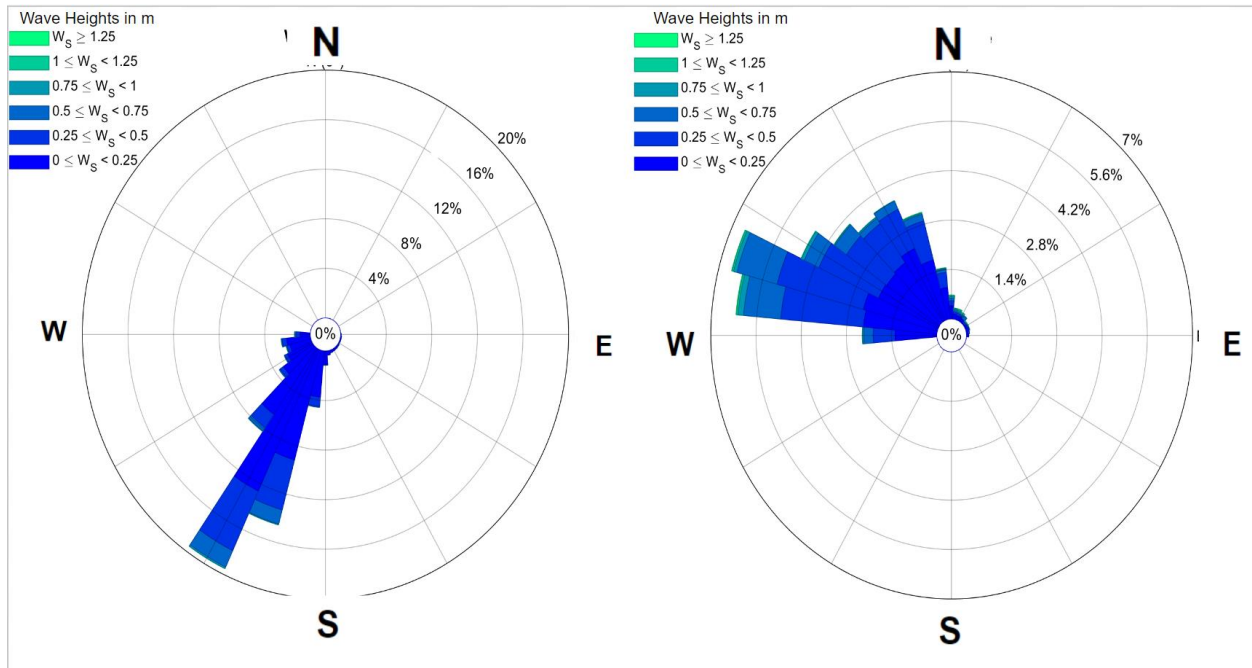


**Figure 9: Wave Roses for CSOTS Overall Averages (for a full year), Separated by Direction. Right Represents Southwest Waves, Left Represents Northwest Waves.**

The wave data's directionality will help to inform testing later, such as testing the WECs at different angles. Angled wave testing is beyond the scope of this thesis but is a suggested area for further research. The Beaufort Sea state number percentage occurrence and the wind and wave directions and intensities, as shown in the above analysis, give a wide lens understanding of what conditions are to be expected in Castine. Once the significant wave heights and peak periods were obtained, a scatter plot was created, and can be seen in Figure 10 in blue. This scatter plot data is then further binned into 0.05 m significant wave height increments, their parameters averaged, and the new points are plotted in Figure 10 in red, and a least squares regression [22] is fitted to the data. The bins used to create the trendline each have margins of error of one standard deviation away from the data point (standard built in for Microsoft Excel) in both significant wave height and peak period. The least squares regression line is used as the characteristic trendline for the test site, which gives a peak period for a given significant wave height, and vice versa. This allows one to take any set of significant wave heights from a given site and find their Castine Scaled Ocean Test Site representative peak periods. The formula for the least squares regression was found to be:

$$H_s = 0.3684T_p - 0.6636 \quad (4)$$

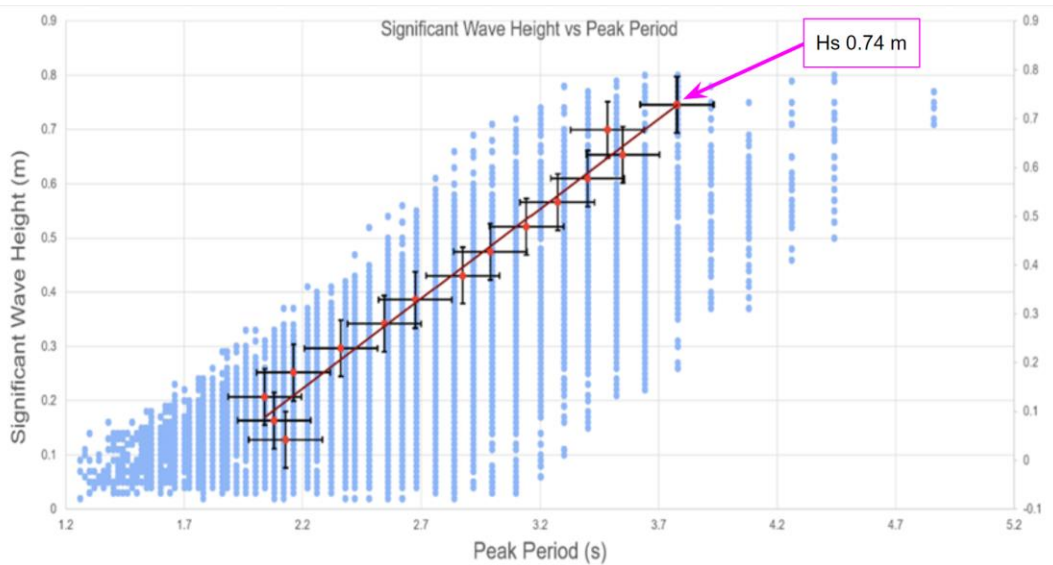
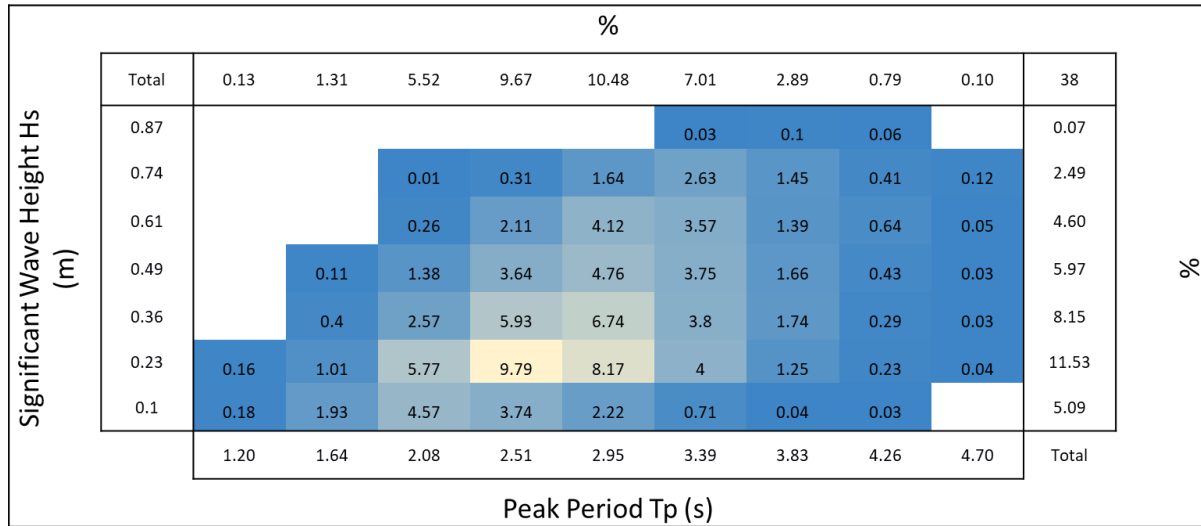


**Figure 10: Significant Wave Height vs Peak Period Scatter plot with Trendline in CSOTS. The blue dots represent data points, while the red dots represent binned averages. A maroon trendline is included for the red dots, and each red dot has error bars in the significant wave height and peak period directions of one standard deviation away from the point. The top binned average significant wave height is identified as 0.74m.**

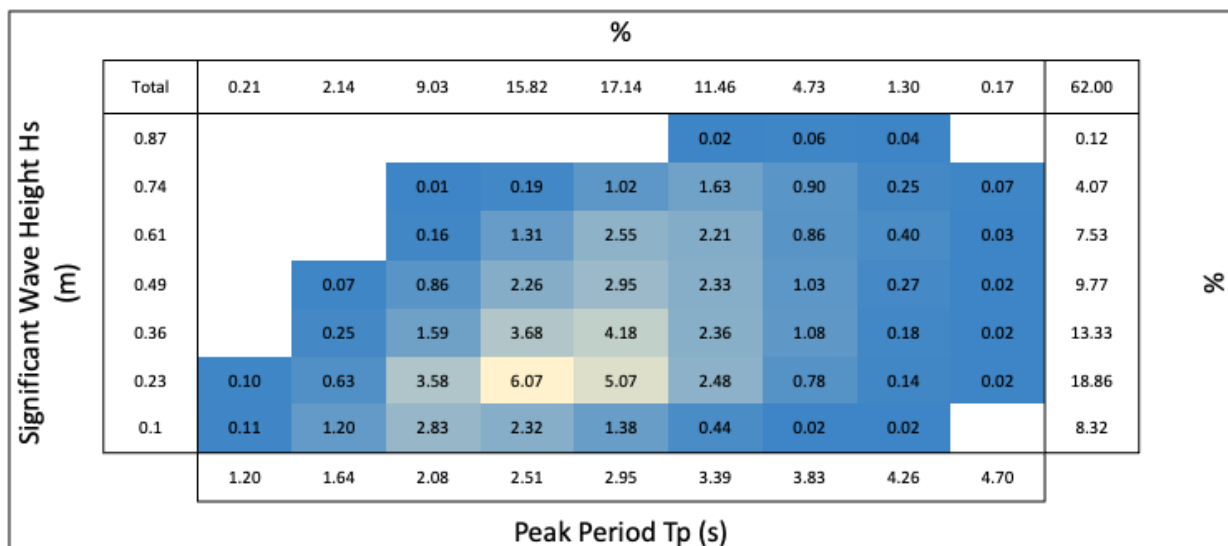
The graph shown in Figure 10 can be made into a heat map, with significant wave heights on the y axis and peak periods on the x axis. Each point in the heat map has a percentage occurrence. This is shown in

Table 7.

**Table 4: CSOTS heat map with significant wave heights on the y axis and peak periods on the left. Percentage occurrence is in each box, with sums of occurrence appearing along the top and right side of the graph.**



Breaking the CSOTS into wave directions, we get the following Figure 11 for the Southwest waves and Figure 12 for the Northwest.



**Figure 11: Southwest wave "heat" map of CSOTS.**



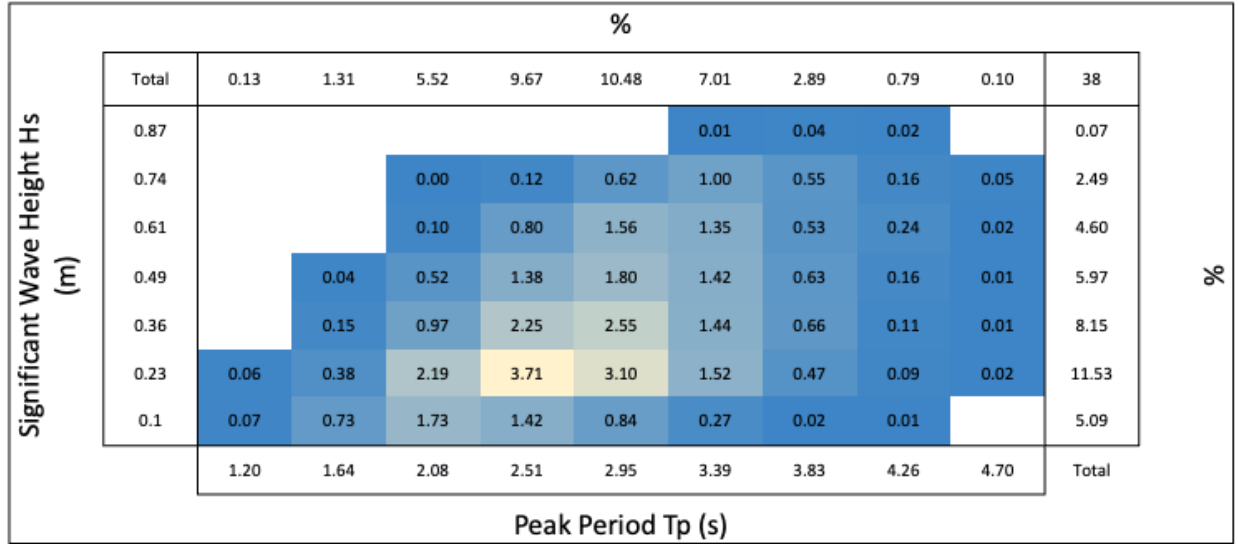


Figure 12: Northwest wave "heat" map of CSOTS.

## 2.4 Implementation of the Method

In this section, the generalized formula for the method described above is presented. To find the scale ratio between any two wave environments of interest, the largest significant wave height is selected from both the desired test site and the original. The quotient of the original test site's maximum significant wave height and the desired test site's maximum significant wave height gives the scaling relationship between the two sites, as shown in the following formula.

$$\lambda_{DTS} = \frac{\text{MAX}(H_{S_{orig}})}{\text{MAX}(H_{S_{DTS}})} \quad (7)$$

Where  $\lambda_{DTS}$  is the scale ratio for the desired test site,  $H_{S_{orig}}$  is the wave height from the original data or full-scale data,  $H_{S_{DTS}}$  is the wave height from the desired test site. Other options for identifying scale ratio may be using the peak periods, most commonly occurring wave, or maximum significant wave heights for specific seasons. Literature on this subject fails to provide a consistent or logical method for finding such a scale ratio, and this method uses frequently identified data in ocean environment characterization to give a scale ratio for any site. This scale ratio can be found for any two sites so long as there is significant wave height data for each.

The scale ratio for the CSOTS for a WEC device was found using the maximum significant wave height from the full-scale Pacific environment, and the maximum significant wave height from the data collected and characterized at the CSOTS. The maximum significant wave height from the full-scale environment was found to be 2.05 m (from the Pacific Coast site), and the maximum significant wave height from CSOTS is 0.74 m which can be seen in Figure 10, in pink. This scale ratio was then calculated as shown:

$$\lambda_{CSOTS} = \frac{1.9 \text{ m}}{0.74 \text{ m}} = 2.5 \quad (5)$$

The result of 2.5 was rounded to a 2:1 scale ratio. The scale ratio when comparing the University of Maine Wind/Wave laboratory basin was found by using the full-scale maximum significant wave height and the basin scale maximum significant wave height. For a basin maximum significant wave height of 0.3, the scale ratio was calculated as follows:

$$\lambda_{DTS} = \frac{2.05 \text{ m}}{0.3 \text{ m}} = 6.83 \quad (6)$$

The result of 6.83 rounds to a basin scale ratio of 7:1.

## 2.5 Applications

In this section, a given percentage occurrence map from the full-scale Pacific Ocean Test site is given (Table 5) and is scaled to CSOTS scale and to the University of Maine's Wind Wave Basin scale using the scale ratios identified previously. These percentage occurrence maps (or heat maps) are characteristic of the environment that they represent, and, once scaled, can be used for accurate scale model testing. Each box in the heat map represents a single wave that corresponds to its significant wave height (left column) and its peak period (bottom row) and shows a percent occurrence in the field. The right column and top row add the percentages of each row and column, respectively. Basin testing is expensive in both cost and time, where each test can take up to 30 minutes with 20 minutes of settling time in between, therefore, 6 waves in the matrix are chosen to best represent the environment. These 6 waves are shown in black boxes. To create the scaled test matrix that is representative of reference place, the trendline from Figure 10 is used to calculate

the scaled peak periods, the significant wave heights are scaled using the scale ratio. Table 6 shows the heat map for CSOTS. The periods from the Pacific Site were scaled to the CSOTS trendline, and the whole map was scaled geometrically by the calculated scale ratio, 1:2. This allows us to find a CSOTS scaled heat map that is informed by the original site, notice that the original CSOTS heat map (Table 4) and the Pacific informed CSOTS map (Table 6) are similar. The basin heat map, shown in Table 5 is at a 1:7 scale, where wave heights and peak periods were scaled geometrically by 1:7. This makes for a CSOTS informed scaled original test site for wave basin testing, where a WEC at 1:7 scale being tested in these conditions in the basin would want its rated wave to be the highest occurring wave.

**Table 5: Full-Scale site probability of occurrence or “heat” map**

		%									
Significant Wave Height Hs (m)	Total	0.13	1.31	5.52	9.67	10.48	7.01	2.89	0.79	0.10	38
	2.03						0.03	0.1	0.06		0.07
	1.89			0.01	0.31	1.64	2.63	1.45	0.41	0.12	2.49
	1.68			0.26	2.11	4.12	3.57	1.39	0.64	0.05	4.60
	1.54		0.11	1.38	3.64	4.76	3.75	1.66	0.43	0.03	5.97
	1.33		0.4	2.57	5.93	6.74	3.8	1.74	0.29	0.03	8.15
	1.19	0.16	1.01	5.77	9.79	8.17	4	1.25	0.23	0.04	11.53
	0.98	0.18	1.93	4.57	3.74	2.22	0.71	0.04	0.03		5.09
		6.42	8.01	9.60	11.19	12.77	14.36	15.95	17.54	19.13	Total
			Peak Period Tp (s)								

**Table 6: 1:2-Scale CSOTS probability of occurrence or “heat” map**

		%									
Significant Wave Height Hs (m)	Total	0.13	1.31	5.52	9.67	10.48	7.01	2.89	0.79	0.10	38
	1.02						0.03	0.1	0.06		0.07
	0.95			0.01	0.31	1.64	2.63	1.45	0.41	0.12	2.49
	0.84			0.26	2.11	4.12	3.57	1.39	0.64	0.05	4.60
	0.77		0.11	1.38	3.64	4.76	3.75	1.66	0.43	0.03	5.97
	0.67		0.4	2.57	5.93	6.74	3.8	1.74	0.29	0.03	8.15
	0.60	0.16	1.01	5.77	9.79	8.17	4	1.25	0.23	0.04	11.53
	0.49	0.18	1.93	4.57	3.74	2.22	0.71	0.04	0.03		5.09
		4.32	4.40	4.47	4.55	4.63	4.70	4.78	4.86	4.93	Total
			Peak Period Tp (s)								

**Table 7: 1:7 Scale Basin probability of occurrence or “heat” map**

		%									
Total		0.13	1.31	5.52	9.67	10.48	7.01	2.89	0.79	0.10	38
Significant Wave Height Hs (m)	0.26						0.03	0.1	<b>0.06</b>		0.07
	0.24			0.01	0.31	<b>1.64</b>	2.63	1.45	0.41	0.12	2.49
	0.22			0.26	2.11	4.12	3.57	1.39	0.64	0.05	4.60
	0.20		0.11	1.38	3.64	4.76	3.75	1.66	0.43	0.03	5.97
	0.19		0.4	2.57	5.93	6.74	3.8	1.74	0.29	0.03	8.15
	0.17	0.16	1.01	5.77	<b>9.79</b>	8.17	4	1.25	0.23	<b>0.04</b>	11.53
	0.15	<b>0.18</b>	1.93	4.57	3.74	2.22	0.71	<b>0.04</b>	0.03		5.09
		2.25	2.31	2.49	2.66	2.84	3.02	3.20	3.37	3.55	Total
		Peak Period Tp (s)									

The waves selected for testing within the heat map are picked to best represent the extremes of the environment. There is a wave that represents the highest occurrence, highest significant wave height, longest peak period, lowest significant wave height, and lowest peak period. Each wave is chosen so that the heat map is accurately represented, and so as not to have too similar wave runs. The most commonly occurring wave will be the wave that generates the most power for the device. A JONSWAP of the most commonly occurring wave is shown in Figure 13.

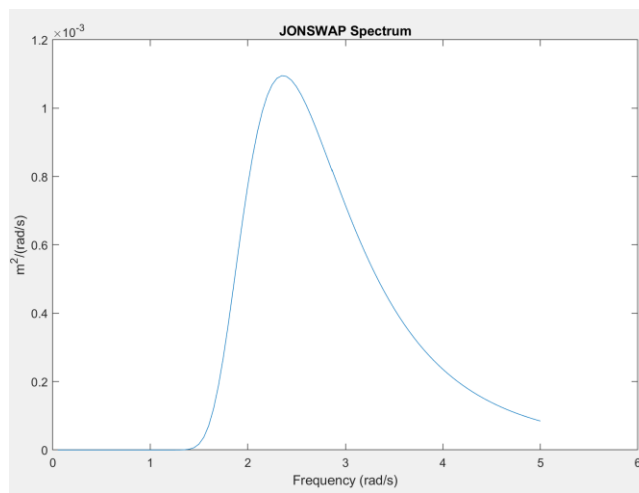


**Figure 13: JONSWAP spectrum graph for most commonly occurring wave in the CSOTS environment with a significant wave height of 0.17m and a peak period of 2.66s, occurring 9.79 percent of the time.**

## 2.6 Discussion

The method described in this chapter defines a consistent method for characterizing a wave environment and identifying a scale ratio to accurately test a scaled wave energy converter. Using this method, the CSOTS wave environment was characterized, and a scale ratio was identified in the equation in section 2.4 .

Scale model testing is used to provide real and accurate data for model validation and can provide insight into how devices behave in harsh conditions, without the high time cost and price tag [5]. These findings will aid in the testing of wave energy converters at the CSOTS, but the methods can be applied to any desired test site for any wave energy converter. A successful demonstration of a scaled device at CSOTS is the VoltturnUS [23] developed by the University of Maine. Figure 14 depicts the VoltturnUS 1:8 at CSOTS in calm sea states and during a scaled 500-year storm event. Calculating extreme storms is outside the scope of this thesis but is beneficial to understand the survival conditions of a device and what type of extreme loads a device will see in its lifetime. The data collected and used in this chapter was obtained over the course of a single year, however, many years' worth of data will offer a better understanding of interannual variations and environmental conditions [13]. It may also be beneficial to review multiple locations and compare scale ratios to identify the most cost effective and or convenient location for scaled ocean testing.



Figure 14: VoltturnUS 1:8 in Scaled Ocean Test Site in calm waters (left) and in an extreme environment (right). [23]

## CHAPTER 3

### Performance and Cost Metrics Development

#### 3.1 Introduction

Performance metrics play an important role in assessing and measuring the effectiveness and success of various endeavors, whether in management [24], shopping [25], sports [26] [27], or renewable energy [28]. Metrics in all areas provide quantifiable and objective information that helps in evaluating progress, identifying areas for improvement, and making informed decisions. By defining straightforward performance metrics, research communities can set goals within their field and evaluate their individual performance based on these standards.

Adequate research goes into the development of metrics to create standards for a research community. One study in the superconductor research space identified the importance of selecting the appropriate measures for volumetric performance of compact capacitors and critiqued the field's access to uniform and standard metrics [29]. Since performance metric literature in this chapter's area of study is also varied, the metrics developed in this chapter of the thesis likewise aim to unify the performance evaluation in wave energy converter development and thus create more value for the research community [29]. Moreover, performance metrics allow stakeholders to understand the effectiveness of new and different technologies whose technical information may have otherwise been inaccessible to them, like this study. Examples of this can be seen in management strategy, where managers can evaluate supply chain management [30] and employee job performance [24]. Similarly, sports fans can use metrics to compare athletes to one another [26], just like how they can be used to compare design variations of a device. Technology is often optimized through the lens of performance metrics, such as developing bin picking systems in Amazon warehouses [25], or managing athlete training to maximize training time and minimize injury risk [27]. Metrics are used to evaluate methods for optimization for multi-objective optimization algorithms [31] [32], like how they will be used in this thesis to optimize WEC hull shape designs.

Performance and cost metrics are critical in the renewable energy sector. Metrics that are standardized, optimizable, straightforward, and comparable are needed to push the renewable energy field into a space that can compete more readily with non-renewable sources. Power production efficiency metrics are heavily used in the offshore wind turbine and farm industry. Some widely used metrics include availability, power generation ratio, and power coefficient, which evaluate the productivity and efficiency of a wind turbine and turbine farm [33]. Metrics that are used to compare the performances of different wave energy converters include absorbed energy per characteristic mass, per characteristic surface area, and per root mean square of Power Take Off (PTO) force [34]. Similarly, performance metrics are used to evaluate and optimize the geometry of a WEC by assessing the hydrodynamic performance, structural reliability, and economic data to avoid problems in late-stage design, like capture width ratio [35]. A study on the optimization of hull geometry of wave energy converters to reduce the cost of creation to advance the technology evaluates the usefulness of many widely used WEC metrics [36].

In this chapter, metrics are developed to optimize the hull shape of a WEC to increase the power generation, reduce forces and moments, and reduce the cost. The hull is the structure with the highest cost reduction potential, and hull geometry optimization has been prioritized for WECs for the last 20 years [36]. This study looks at evaluation metrics commonly used for WEC performance (specifically with respect to hull geometry), such as annual energy production, mean power, efficiency based on radiation field, capture width and capture width ratio, and more [36]. The outputs of these studies must be comparable, and these metrics aim to amalgamate the plethora of evaluation metrics that exist, while also providing metrics unique to the testing goals in this study.

Originally suggested for the performance metrics in this study were the U.S. Department of Energy's Wave Energy Prize Competition's average capture width (ACCW) to characteristic capital expenditure (CCE), otherwise known as ACE metric. This metric was proposed for the wave energy prize competition as a replacement of the levelized cost of energy (LCOE) [37] for low technology readiness level (low-TRL) WECs. LCOE's extensive need for device information such as assumed lifetime and annual average electricity generation values creates obstacles for new technologies that have uncertainty in design and operation [38].

Although the ACE metric was a combination of widely used metrics in the Wave Energy Converter field such as capture width ratio and LCOE, many WEC manufacturers and researchers refuse to use it as a measure of their design effectiveness because it doesn't account for device performance characteristics that would usually affect LCOE and gives drastically high values for small changes in material cost. The need for better design metrics for early-stage devices is clear.

### **3.2 Current Industry Used Metrics**

Current WEC metrics can be found in an NREL-created Portal and Repository or Information on Marine Renewable Energy (PRIMRE) [28], such as ACE and LCOE. Many of these metrics assess the performance of WECs through levelized costs (LCOE), energy production (capacity factor, availability), strength (mean time to failure), or time to install (mean time to install). These metrics are useful for well-developed and well-documented technologies, but metrics for preliminary design may be more useful for this chapter's application. Existing low-TRL metrics, such as material construction cost (MCC), ACE, technology performance level, power-to-weight ratio, etc. are useful in their own ways, but were found to be either irrelevant to this chapter's application or difficult to calculate. MCC, for example, is a very crude measure of cost; a good estimate for the cost to produce a part that is more than just cost per pound of material is needed. Some of the current metrics can be modified to fit the current application, such as the power-to-weight ratio (PWR). PWR is the product of the rated power of the device and the capacity factor over the mass of the system. Since low-TRL devices have limited access to capacity factor information, and to make it more comparable to the other metrics in this development, our mass per energy production (MPE) metric was developed.

### **3.3 Justification and Overview of Developed Metrics**

The metrics available on PRIMRE are useful metrics in their own way, but new metrics are needed for the specific scenarios addressed for this project's test campaign and low-TRL devices. The metrics developed



in this chapter are for three different WEC evaluation scenarios. Scenario one involves power production of different component designs as used for hull geometry shape, in example. Scenario two includes force and moment testing of different component designs as used for components that may experience higher forces such as mooring lines, appendages, and structural members that are of high interest to optimize. For this study, the component of interest was a proprietary design and cannot be discussed. Scenario three is the material cost evaluation of different component designs for different manufacturing processes such as additive manufacturing of components so as to optimize the component fabrication methods. The metrics were designed to assess the performance of each WEC device by iterating the design and/or material of a single component. For scenario one, the design iterations are that of the hull geometry shapes. Scenario two's design iteration is in the LTU tower geometry. Scenario three involves iterating through different materials. Each scenario will be evaluated using metrics created specifically for comparing iterations of the same device, and devices will not be cross compared. One important tool when making generic metrics that allow for comparison from design iteration to design iteration is normalization to the baseline design, which is done for most metrics discussed in this chapter. Finally, to help to calculate a LCOE, this analysis will utilize a tool from NREL called the System Advisor Model (SAM) [39].

### **3.3.1 Geometry Optimization for Power Production Metrics**

This section describes the calculations of the performance evaluation metrics for WEC devices looking to optimize components for power production in their rated environments. Specifically, one WEC company wanted to optimize their hull shape for power production, so the proposed metrics needed to measure power production for each iteration. The proposed metrics and their descriptions are as follows:

1. Normalized Energy Production (NEP) is the ratio of the mean energy production over mean energy production of the baseline.
2. Normalized Component Mass (NCM) is the ratio of the full-scale modified component mass compared to the baseline component mass.

3. Normalized Component Cost (NCC) is the ratio of the estimated construction cost of components of interest in a design iteration over the estimated cost of construction of the baseline and is dependent on the material used to make the component.
4. Mass Per Energy Production (MPE) is calculated by the component mass divided by the weighted energy produced (either the NEP or energy production without normalization) summed over each sea state.
5. SAM marine energy performance model coupled with LCOE Calculator Financial Model. The NREL System Advisor Model (SAM) is used to calculate LCOE. SAM couples its Marine Energy Wave Model with the LCOE Calculator Financial Model. The LCOE calculations focus on system costs estimates that are available for a system under early development. The SAM energy production estimation for the WEC device can be calculated as rated power times capacity factor. Since the component would perform functionally the same as far as power production, the power production calculations should be constant for all variants.

### 3.3.1.1 Normalized Energy Production (NEP)

Normalized Energy Production (NEP) is the average energy produced by the geometry design iteration over the average energy produced by the baseline design. This metric indicates the performance of a component geometry design iteration compared to the baseline under the same sea states. An NEP greater than 1.0 means that the variant case creates more energy due to an ocean environment than that of the baseline. An NEP less than 1.0 means that the variant creates less power due to a given wave environment than the baseline. The energy production measurement used in this calculation may be measured at scale but should be evaluated at full scale. The NEP is calculated as follows.

$$NEP^j = \frac{EP_{avg}^j}{EP_{avg\ base}^j} \quad (7)$$

Where  $NEP^j$  is the normalized energy produced from sea state  $j$ ,  $EP_{avg}^j$  is the average energy produced for sea state  $j$ , and the *base* subscript denotes the baseline design. This metric can be weighted by a sea state weight (or percentage occurrence) between zero and 1 (the sum of which over all sea states adds up to 1). This weighted NEP is as follows.

$$NEP_{weighted} = \sum NEP^j \times \mathcal{E}^j \quad (8)$$

Where  $NEP_{weighted}$  is the sea state weighted NEP, and  $\mathcal{E}^j$  is the sea state weight or percentage occurrence for sea state  $j$ .

### 3.3.1.2 Normalized Component Mass (NCM)

The Normalized Component Mass (NCM) is the mass of the component of interest design iteration over the mass of the baseline component. This metric indicates the mass change from the baseline to the design iteration. A normalized component mass greater than 1 means that the variant has more mass than that of the baseline. A NCM less than 1 means that the variant has less mass than the baseline. This metric is used to compare variants of different shapes and materials. An NCM that is far greater or far less than 1 may indicate that the mooring pretension may need to change to account for a different buoyancy of the whole WEC due to mass changes.

The NCM metric is calculated by taking the surface area and thickness of the component design iteration and baseline design for the calculation of a volume. The volume is then multiplied by the respective material density that the component is being made from (considering that a 3D printed materials' density is dependent on the percent infill selected for the printing process and can be taken from the slicing software of the 3D printer being used). The mass of the component iteration is then divided by the mass of the baseline component. The calculation of the NCM is as follows.

$$NCM = \frac{A_s \cdot t \cdot \rho}{(A_s \cdot t \cdot \rho)_{base}} = \frac{Mass}{Mass_{base}} \quad (9)$$

Where  $A_s$  is the surface area of the component,  $t$  is the wall thickness of the component,  $\rho$  is the density of the component material, the *base* subscript denotes the baseline case, and  $Mass$  is the mass of the component.

### 3.3.1.3 Normalized Component Cost (NCC)

The Normalized Component Cost (NCC) is the total cost of the labor, material, and manufacturing of a component over the same costs for the baseline component. The NCC is an indicator of how much more or less expensive a new design iteration is to create compared to the baseline. The NCC is the sum of labor cost, material cost, and manufacturing cost over the summed costs of the baseline:

$$NCC = \frac{\Sigma(Cost_{labor} + Cost_{material} + Cost_{manufacturing})}{\Sigma(Cost_{labor} + Cost_{material} + Cost_{manufacturing})_{base}} \quad (10)$$

Where  $Cost_{labor}$  could include the following factors.

- Costs for the personnel that design the component.
- Costs for the personnel that create the computer model design.
- Costs for the personnel that manufacture the design.

Where  $Cost_{material}$  could include the following factors.

- Costs of the material used in the design.
- Costs for the material shipping and handling.
- Costs for the materials that connect component to hull (screws, welding, etc.).

Where  $Cost_{manufacturing}$  could include the following factors.

- Costs for use time of the 3D printers.
- Costs for use time of CNC or machining devices used.

Where the subscript *Base* denotes baseline case.

#### **3.3.1.4 Mass Per Energy Production (MPE)**

Mass per Energy Production is calculated by dividing the NCM (Section 3.3.1.2 ) by the weighted NEP (Section 5) This metric is useful in determining component iteration performance, and how it fares to the baseline. A higher Mass per Energy Production indicates a less efficient design, while a lower Mass per Energy Production indicates a more efficient design. Mass per Energy Production for an individual iteration is calculated by the NCM divided by the weighted NEP.

$$MPE = \frac{NCM}{NEP_{weighted}} \quad (11)$$

Where *MPE* is the mass per energy production.

#### **3.3.1.5 SAM Marine Energy Performance Model for LCOE**

The NREL System Advisor Model (SAM) [39] can be used to calculate the LCOE. SAM couples its Marine Energy Wave Model with the LCOE Calculator Financial Model. The LCOE calculations for additive manufacturing should focus on system cost estimates that are available for a system under early development. The SAM evaluation of LCOE for component design uses estimates for energy production for the WEC device such as rated power times capacity factor. Since the component would perform functionally the same as far as power production, the power production calculations should be constant for all variants.

The inputs required for the SAM model include:

- Wave height versus wave period table to characterize the wave resource. This can also be a time series of wave records over a year at the location of interest.
- The performance parameters for the wave energy converter.
- Specifications of the positions of each WEC device in an array, which can be as few as 1.
- Data specifying expected losses. This can be set to zero if more data is not available.

- Installation and operating costs for LCOE calculations. This can be set to zero if more data is not available.
- Financial parameters for LCOE calculations such as structural component costs and manufacturing costs.

### **3.3.2 Geometry Optimization Metrics for Component Force and Moment Reduction**

This section describes the calculations of the performance evaluation metrics for WEC devices looking to optimize components that may be subjected to high forces and fatigue loads, such as 5-, 10-, or 50-year storms and higher. The proposed metrics include:

1. Normalized Force (NF) is the ratio of the weighted absolute value average force on the component iteration over the weighted absolute value average force on the baseline tower design.
2. Normalized Moment (NM) is the ratio of the component iteration bending moment over the baseline case.
3. Normalized Component Mass (NCM) is the ratio of the full scale modified component mass compared to the baseline component mass. (Seen in section 3.3.1.2 )
4. Normalized Component Cost (NCC) is the ratio of the estimated construction cost of components of interest in a design iteration over the estimated cost of construction of the baseline and is dependent on the material used to make the component. (Section 3.3.1.3 ).
5. Mass per Force (MPF) is the component mass over the average absolute value force.
6. Mass per Moment (MPM) is the component mass over the average absolute value force.

#### **3.3.2.1 Normalized Force (NF)**

Normalized Force (NF) is the average absolute value force on a component design iteration over the average absolute value force on the component design baseline. Forces of interest for this metric may

include shear force or axial force, for example. This metric indicates the performance of the design iteration under the same sea states with respect to the baseline. A NF greater than 1.0 means that the variant case takes on more force due to an ocean environment than that of the baseline. A NF of less than 1.0 means that the variant experiences less force due to a given wave environment than the baseline. The NF is calculated as follows:

$$NF^j = \frac{|F^j|_{avg}}{|F^j|_{avg_{base}}} \quad (12)$$

Where  $NF^j$  is the NF for sea state  $j$ ,  $|F^j|_{avg}$  is the average absolute value for sea state  $j$ , and  $|F^j|_{avg_{base}}$  is the absolute value of the average force for the baseline for sea state  $j$ . This metric can be weighted by a sea state weight (or percent occurrence) between 0 and 1 (the sum of which over all sea states adds up to 1).

This weighted NF is:

$$NF_{weighted} = \sum NF^j \times \mathcal{E}^j \quad (13)$$

Where  $NF_{weighted}$  is the sea state weighted NF, and  $\mathcal{E}^j$  is the sea state weight for sea state  $j$  (probability of sea state occurrence).

### 3.3.2.2 Normalized Moment (NM)

The Normalized Moment (NM) is the average absolute value bending moment of a WEC component design iteration over the average absolute value bending moment of the baseline design. This bending moment can be at the base of an appendage or within the hull, for example. This metric indicates the performance of a component design iteration compared to the baseline design under the same sea states. A NM greater than 1 means that the variant case takes on more bending moment stress due to an ocean environment than that of the baseline. A NM less than 1 means that the variant experiences less bending moment stress due to a given wave environment than the baseline. The NM is calculated as follows:

$$NM^j = \frac{|M^j|_{avg}}{|M^j|_{avg_{base}}} \quad (14)$$

Where  $NM^j$  is the NM for sea state  $j$ ,  $|M^j|_{avg}$  is the average absolute value for sea state  $j$ , and  $|M^j|_{avg_{base}}$  is the absolute value of the average moment for the baseline for sea state  $j$ . This metric can be weighted by a sea state weight (or percent occurrence) between 0 and 1 (the sum of which over all sea states adds up to 1). This weighted NM is:

$$NM_{weighted} = \sum NM^j \times \mathcal{E}^j \quad (15)$$

Where  $NM_{weighted}$  is the sea state weighted NM, and  $\mathcal{E}^j$  is the sea state weight for sea state  $j$  (probability of sea state occurrence).

### 3.3.2.3 Mass Per Force (MPF)

The Mass per Force (MPF) is calculated by dividing the NCM (NCM, section 3.3.1.2 ) by the weighted NF (section 3.3.2.1 ). This metric is useful in determining component iteration endurance, and how it fares to the baseline. A higher MPF indicates a more rugged design, while a lower MPF indicates a less rugged design that may have a shorter lifespan. When normalized to the baseline, an MPF less than 1.0 means that the variant component is more rugged than the baseline, and an MPF greater than 1.0 indicates that the baseline is more rugged. MPF for an individual iteration is calculated by the NCM (section 3.3.1.2 ) divided by the weighted NM summed over each sea state. The MPF for an individual iteration is calculated by the NCM divided by the weighted NF summer over each sea state.



$$MPF = \frac{NCM}{NF_{weighted}} \quad (16)$$

Where *MPF* is the Mass per Force.

### 3.3.2.4 Mass per Moment (MPM)

Mass per moment is calculated by dividing NCM (section 3.3.1.2 ) by the weighted NM (section 3.3.2.2 ). This metric is useful in determining component iteration endurance, and how it fares to the baseline. A higher MPM indicates a more rugged design, while a lower MPM indicates a less rugged design that may have a shorter lifespan. When normalized to the baseline, a MPM greater than 1.0 means that the variant component is more rugged than the baseline, where a MPM less than 1.0 indicates that the baseline is more rugged. MPM for an individual iteration is calculated by the NCM divided by the weighted NM summed over each sea state.

$$MPM = \frac{NCM}{NM_{weighted}} \quad (17)$$

Where *MPM* is the Mass per Moment.

### 3.3.3 Additive Manufacturing Metrics

This section describes the calculations of the performance evaluation metrics for the additive material construction of WEC components. In addition to these metrics, to calculate the LCOE, the System Advisor Model (SAM) [39], developed by NREL, is used. SAM's marine energy performance model is coupled with the LCOE Calculator financial model to quantify the LCOE. The proposed metrics in this section include:

6. Normalized Component Mass (NCM) is the ratio of the full-scale component mass compared to the baseline mass, see section 3.3.1.2 .

7. Normalized Component Cost (NCC) is the ratio of the estimated construction cost of components of interest in a design iteration over the estimated cost of construction of the baseline and is dependent on the material used to make the component. See section 3.3.1.3 .
8. SAM marine energy performance model coupled with LCOE Calculator Financial Model. (See Section 3.3.1.5 )

### **3.4 Discussion of Metrics**

The NEP, MPE, NCM, NCC, and SAM LCOE all make for metrics that can help to evaluate and optimize hull performance for energy production. Another metric that could be formulated is the cost per energy production, but this was used because mass is more accurately measured, and costs at early stages are not as well known. For early-stage development, cost is going to be limited and possibly inaccurate, but normalizing the cost metric allows for the baseline and variants to be evaluated using the same availability of data and therefore improves the use of the metric. Additionally, LCOE is desired, but since it is not normalized, it requires accurate information about energy production and about the costs of the components, this is rarely the case with the LTR designs in this study, therefore the previous metrics become more important in evaluating the performance of designs relative to a baseline.

The above sections detail the modifications of existing metrics that are currently used in industry so that they more accurately measure the goals of the tests being performed, such as hull geometry optimization for power production, tower design optimization for force and moment measurements, and additive manufacturing cost analysis. Each metric, when possible, is normalized to a baseline to make results more comparable and unitless. These metrics have been created to reflect performance more accurately while the technology is still in the early stages of development, like the SAM model. Since the technology is new, it is hard to get a truly accurate estimate of performance; a lifespan measurement would be useful, especially when calculating LCOE. Unfortunately, lifespan measurements are impossible to assess in a month-long test with novel materials that have little fatigue data.

### 3.5 Example Calculations

Example calculations are shown in Figure 15 and Figure 16. Figure 15 shows the spreadsheet that calculates weighted average force and weighted average moment, which are values that go into NF and NM calculations, from baseline design testing outputs. Included in this figure are sea state weights, and normalized sea state weights (where sea states are normalized to add up to 100% of the 6 chosen sea states). The forces and moments are directly from measurements. As described previously, the force and moment reduction scenario testing are in more extreme environments and is a scaled-up version of the original 1:7 basin test matrix. It should also be noted that the weighting calculation is done before the normalizing of the metric, which is different from the above descriptions. This weighting calculation can be done either way but should only be done once.

Baseline		Sea State 1 (SS1)		Sea State 2 (SS2)		Sea State 3 (SS3)		Sea State 4 (SS4)		Sea State 5 (SS5)	
		WC-14 Hs 0.275m Tp 2.702s		WC-18 Hs 0.275m Tp 2.446s		WC-19 Hs 0.158m Tp 1.680s		WC-16 Hs 0.383m Tp 2.976s		WC-15 Hs 0.290m Tp 2.337s	
		Tower Force [N]	Tower Base Bending Moment [N*m]	Tower Force [N]	Tower Base Bending Moment [N*m]	Tower Force [N]	Tower Base Bending Moment [N*m]	Tower Force [N]	Tower Base Bending Moment [N*m]	Tower Force [N]	Tower Base Bending Moment [N*m]
Sea State 1 Weight	15.40%	-10.494	-0.831	-9.621	-0.851	-6.434	-0.878	-9.438	-0.834	-7.374	-0.6
Sea State 2 Weight	44.16%	-10.469	-0.843	-9.957	-0.856	-8.027	-0.88	-10.168	-0.827	-7.205	-0.58
Sea State 3 Weight	1.67%	-10.335	-0.829	-9.487	-0.871	-7.828	-0.839	-9.295	-0.817	-8.681	-0.576
Sea State 4 Weight	0.56%	-10.487	-0.833	-9.875	-0.862	-8.199	-0.86	-9.758	-0.832	-7.57	-0.612
Sea State 5 Weight	38.22%	-10.592	-0.839	-9.163	-0.852	-6.845	-0.867	-10.05	-0.836	-7.435	-0.622
		-10.098	-0.832	-9.617	-0.836	-6.922	-0.88	-10.168	-0.825	-6.868	-0.619
		-10.906	-0.828	-9.845	-0.838	-7.79	-0.876	-9.314	-0.812	-7.889	-0.619
Weighted Average Force	8.73964	-10.694	-0.824	-9.72	-0.847	-7.136	-0.84	-10.293	-0.808	-6.867	-0.643
Weighted Average Moment	0.77878	-10.358	-0.81	-10.174	-0.866	-6.897	-0.82	-9.874	-0.823	-7.923	-0.663
		-10.529	-0.795	-9.688	-0.859	-6.795	-0.843	-9.393	-0.82	-6.744	-0.662
		-10.876	-0.801	-9.702	-0.852	-7.124	-0.872	-9.908	-0.803	-6.519	-0.661
		-10.174	-0.823	-9.307	-0.853	-7.1	-0.875	-9.704	-0.821	-7.421	-0.673
		-10.721	-0.832	-9.633	-0.858	-7.397	-0.851	-10.063	-0.831	-5.907	-0.662
Non Normalized Weights		-10.443	-0.817	-9.312	-0.855	-5.559	-0.839	-9.488	-0.829	-6.783	-0.658
Sea State 1 Weight	1.66	-10.631	-0.807	-9.624	-0.847	-7.649	-0.822	-10.021	-0.805	-6.797	-0.651
Sea State 2 Weight	4.76	-10.653	-0.806	-9.612	-0.867	-6.893	-0.872	-10.525	-0.835	-6.374	-0.671
Sea State 3 Weight	0.18	-10.618	-0.809	-9.803	-0.853	-6.017	-0.889	-9.401	-0.831	-6.642	-0.691
Sea State 4 Weight	0.06	-10.444	-0.814	-9.893	-0.857	-6.666	-0.848	-9.295	-0.839	-6.757	-0.686
Sea State 5 Weight	4.12	-10.526	-0.812	-9.603	-0.862	-6.536	-0.84	-10.851	-0.829	-6.554	-0.669
		-10.437	-0.807	-9.769	-0.871	-6.393	-0.852	-9.085	-0.83	-6.508	-0.649
		-10.149	-0.811	-9.537	-0.848	-6.879	-0.889	-9.8	-0.829	-5.374	-0.654
		-10.728	-0.813	-9.336	-0.86	-6.992	-0.917	-10.368	-0.819	-5.672	-0.663

Figure 15: Spreadsheet that calculates weighted average force and weighted average moment from baseline testing outputs.

## Normalized Component Mass (NCM) and Normalized Component Cost (NCC)

Tower - Baseline			Tower - Mod 1			Tower - Mod 2		
Labor Cost	\$	1000	Labor Cost	\$	1000	Labor Cost	\$	1000
Additive Manufacturing Cost	\$	1000	Additive Manufacturing Cost	\$	1000	Additive Manufacturing Cost	\$	1000
Surface Area	m <sup>2</sup>	2	Surface Area	m <sup>2</sup>	2	Surface Area	m <sup>2</sup>	2
Thickness	m	0.01	Thickness	m	0.01	Thickness	m	0.01
<b>Material</b>	-	<b>Steel</b>	<b>Material</b>	-	<b>Steel</b>	<b>Material</b>	-	<b>Steel</b>
Material Density	kg/m <sup>3</sup>	8000	Material Density	kg/m <sup>3</sup>	8000	Material Density	kg/m <sup>3</sup>	8000
Material Cost	\$	1000	Material Cost	\$	1000	Material Cost	\$	1000
Volume	m <sup>3</sup>	0.02	Volume	m <sup>3</sup>	0.02	Volume	m <sup>3</sup>	0.02
Mass	kg	160	Mass	kg	160	Mass	kg	160
Normalized Component Mass (NCM)	unitless	1	Normalized Component Mass (NCM)	unitless	1	Normalized Component Mass (NCM)	unitless	1
Cost	\$	\$3,000	Cost	\$	\$3,000	Cost	\$	\$3,000
Normalized Component Cost (NCC)	unitless	1	Normalized Component Cost (NCC)	unitless	1	Normalized Component Cost (NCC)	unitless	1

**Figure 16: NCM and normalized component cost calculator spreadsheet.**

## CHAPTER 4

### Potential Flow and Dynamic Model Workflow for Model Validation of WECs

#### 4.1 Introduction

To model the dynamic behavior of a WEC in waves for model validation before fabrication, two types of dynamic system models can be developed, each of which use force coefficients derived from an additional potential flow modeler for each variant. One is a simplified frequency domain model, which estimates average power generation given a wave climate and can help to extract optimal design parameters such as PTO damping coefficients for maximum power generation. The other is a time domain model, which can help to model power production over time. The potential flow model – an open-source code NEMOH [40] is used – computes coefficients for a given geometry of a WEC that can be applied to a single point in the dynamic models. Other potential flow codes, such as WAMIT and Orcaflex are used for potential flow calculations but are expensive to use and not as easily accessible. Time domain models also exist, such as open-source code WEC-Sim (Wave Energy Converter Simulator) [41], which are used for experimental validation, device modeling, and control modeling. Additionally, WEC-Sim is equipped for PTO modeling of WECs, which is essential for this chapter's purpose. Figure 17 shows the schematic to be modeled, where the WEC hull is shown in pink. The PTO is modeled as a winch attached to the WEC and secured by an anchor. A load cell is attached to the mooring.

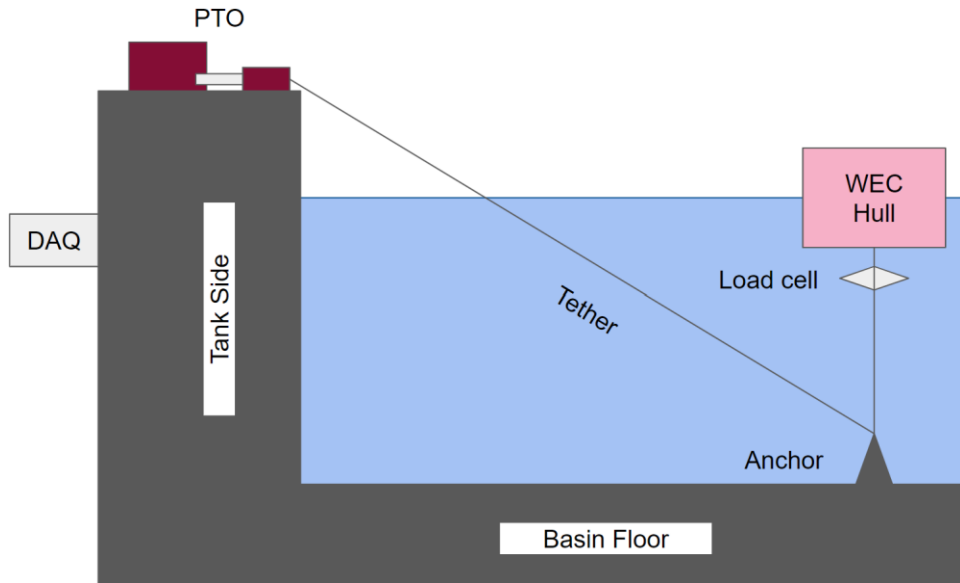


Figure 17: Basin schematic for modeling visual.

The chapter will be organized as follows. A discussion about the potential flow model, the theory and methodology it uses, and its implications is presented first. Then, a similarly set up section on the frequency domain model. Finally, the same for the time domain model. It is important to note that the purpose of this chapter is to describe a WEC modeling workflow using existing tools, and that these tools were not developed for this research. This thesis uses the convention shown in Figure 18 for the positioning and orientation of the global coordinate system (left), from WEC-Sim [41], and the numbering convention for reference in equations and matrices (right). This convention is the same as the most common convention used in naval architecture and specifically in wave energy conversion related research and development.

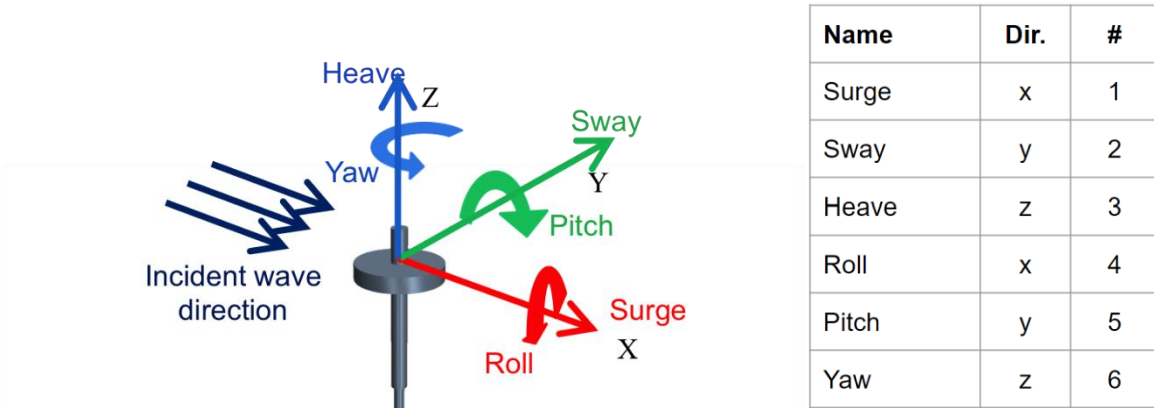
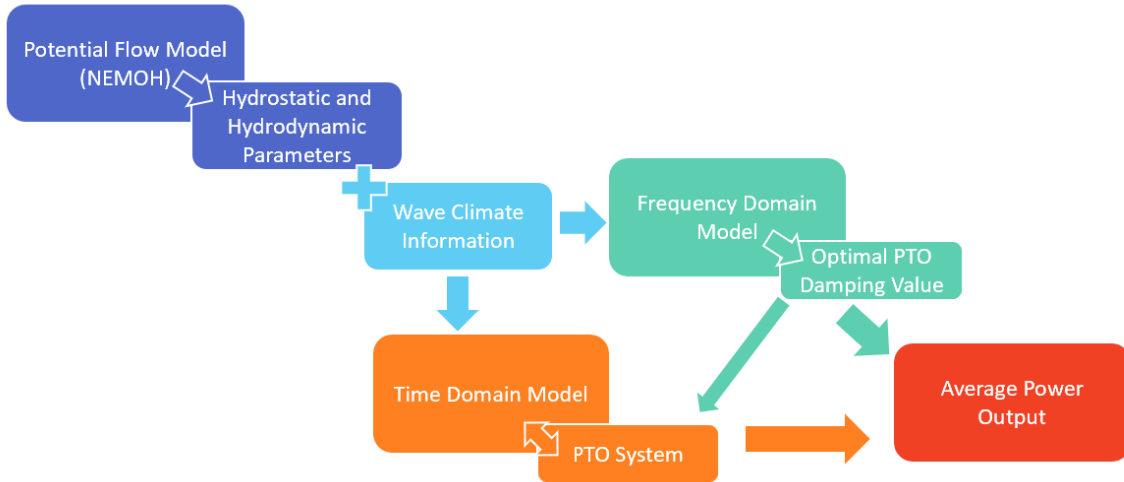


Figure 18: Global Coordinate System and Orientation used throughout this thesis. [41]

Each model has an important place in the research and development of early-stage devices. The potential flow model provides model information such as hydrostatic and hydrodynamic coefficients, which are used by the frequency and time domain models. The frequency domain model takes the potential flow information and calculates motions in the frequency domain and power outputs based on PTO damping values to help to identify the optimal PTO damping values, and to give an estimate of the expected power output of the device given a desired JONSWAP environment. The time domain model also takes the potential flow information and can be given the optimal PTO damping value found from the frequency domain model and gives an estimate of the expected power output of the device given a desired JONSWAP environment in a time-series format.

A flowchart for the workflow created in this chapter is shown in Figure 19. First, the desired WEC hull geometry is modeled in the potential flow model (NEMOH is used), the outputs of which are used as inputs to the frequency and time domain models, along with a prescribed wave environment. The time domain model also includes a control strategy for the PTO which the frequency domain model does not have. These models were used at full scale.



**Figure 19: Flow Chart of Generic Time Domain Model from Input of Potential Flow Model Geometry Definition and Hydrostatic/Hydrodynamic Values (NEMOH) to Frequency Domain Model, to Dynamic Time Domain Model (WEC-Sim) that Gives Power Output for Device.**

#### 4.2 Potential Flow Model

A major effort of this thesis was setting up the potential flow model for WEC hull geometry to use as an input to the dynamic models. The full potential flow theory can be found in the WAMIT [42] and NEMOH [40] user manuals, but the important outputs from the potential flow model that are used in the other models are shown in the following subsections. Since this is a single degree of freedom system, pitch, roll, and yaw, surge, and sway are equal to 0 and their effects on other coefficients are also 0. This means that the coefficients of interest are located at  $i, j = 3$  (heave) in the stiffness matrix (refer to Figure 18). For a WEC, energy is produced by radiation to absorb all the energy of the incoming wave [43]. Determining the right radiation and excitation loads on the body is typically done with boundary element methods (BEMs), which is what the potential model uses. The numerical modelling produced by such BEM codes, such as NEMOH, is based on Newton’s second law, where the inertial force is balanced by all forces acting on the WEC [43]. Such forces are split into external loads and reaction forces (hydrodynamic and hydrostatic). The external loads are:

- Hydrostatic force, which is caused by a variation in the hydrostatic pressure distribution from the oscillatory motion of the body.



- Excitation loads, caused by the incident waves on the body (when motionless).
- Radiation force, which is the force experienced by the body from the variation in the water pressure due to the body's own movement in the water that causes fluid displacement (with no external loads).

Reaction forces include:

- Power take-off (PTO) equipment forces, which is what converts mechanical energy into electrical.
- Mooring system forces, which moors the WEC in place.
- End-stop mechanism, which is used to dissipate the kinetic energy of the body at the peaks of its motion to avoid damage.

The power absorbed by a WEC is related to the power in the PTO damper during a wave. The power in a damper is expressed in Section 4.3 which covers the frequency domain model. The following subsections explain the calculations of some of the necessary quantities from the BEM code that are used in the dynamic models.

#### 4.2.1 Added Mass and Damping Coefficients

The added mass and damping coefficients are defined as follows:

$$A_{ij} - \frac{i}{\omega} B_{ij} = \rho \iint_{S_b} n_i \varphi_j dS \quad (18)$$

Where  $k = 3$  for  $(i, j = 1, 2, 3)$ ,  $k = 4$  for  $(i = 1, 2, 3, j = 4, 5, 6)$ , and  $k = 5$  for  $(i, j = 4, 5, 6)$ ,  $\rho$  is the density of the surrounding fluid (water),  $\varphi_j$  is the velocity potential,  $n_i$  is the normal vector of the degree of freedom of interest (heave),  $S_b$  is the body surface boundary,  $\omega$  is the circular frequency of the incident wave,  $A_{ij}$  is the added mass coefficient, and  $B_{ij}$  is the damping coefficient.

#### 4.2.2 Excitation Forces

WAMIT uses two different kinds of calculations for the excitation forces ( $X_i$ ). One is from the Haskind relations:

$$X_i = -i\omega\rho \iint_{S_b} \left( n_i\varphi_0 - \varphi_i \frac{\partial\varphi_0}{\partial n} \right) dS \quad (19)$$

Where  $\omega$  is frequency,  $\rho$  is density of the fluid,  $n_i$  is the unit normal,  $S$  is the surface boundary, and  $\varphi_i$  is the velocity potential. The other kind of calculation or the excitation forces is direct integration of hydrodynamic pressure:

$$X_i = -i\omega\rho \iint_{S_b} n_i\varphi_D dS \quad (20)$$

Where  $m = 2$  for  $i = 1,2,3$  and  $m = 3$  for  $i = 4,5,6$ . More information about these calculations can be found in [42].

#### 4.2.3 NEMOH Workflow

Figure 20 shows the flow chart of a potential flow solver such as NEMOH, with inputs of the geometry and boundary conditions, calculation of the hydrostatic parameters, computation of the boundary value problems for diffraction potential and radiation potential, and calculation of the hydrodynamic coefficients used in the dynamic models.

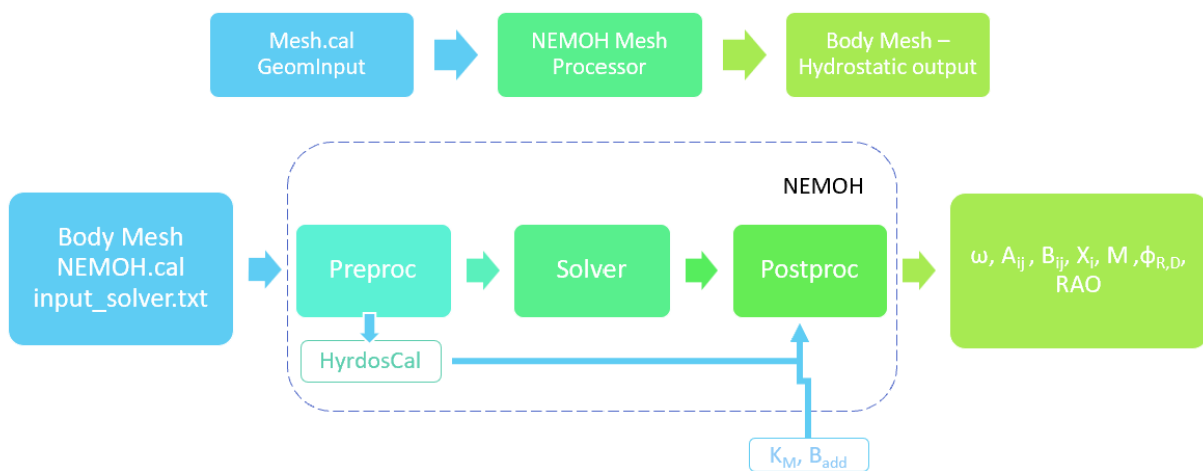


Figure 20: Schematic of Potential Flow Calculation Showing the Methodology Behind Potential Flow.

NEMOH takes a geometry input and creates a mesh and hydrostatic data output and solves for various hydrodynamic quantities at single frequencies for a prescribed range of frequencies. There are four modules: module one (preProc) creates the mesh file and unit surface normals. Module 2 (hydrosCal) calculates hydrostatic parameters such as the stiffness matrix and the inertia matrix. Module 3 (Solver) solves the boundary value problems as defined in NEMOH's user manual [40]. Module 4 (postProc) takes Module 3's output files to give excitation forces, added mass, and damping coefficients, as well as optionally computing response amplitude operators (RAOs) given an additional stiffness matrix ( $K_M$ ), and damping matrix ( $B_{add}$ ). NEMOH's output files include a Froude-Krylov forces file (FKForce.tec), a diffraction forces file (DiffractionForce.tec), an excitation forces file (ExcitationForce.tec), and an added mass and damping coefficients file (RadiationCoefficients.tec) [40]. NEMOH calculates these outputs with user input frequencies that include a "zero" and "infinite" frequency, along with the desired range of frequencies.

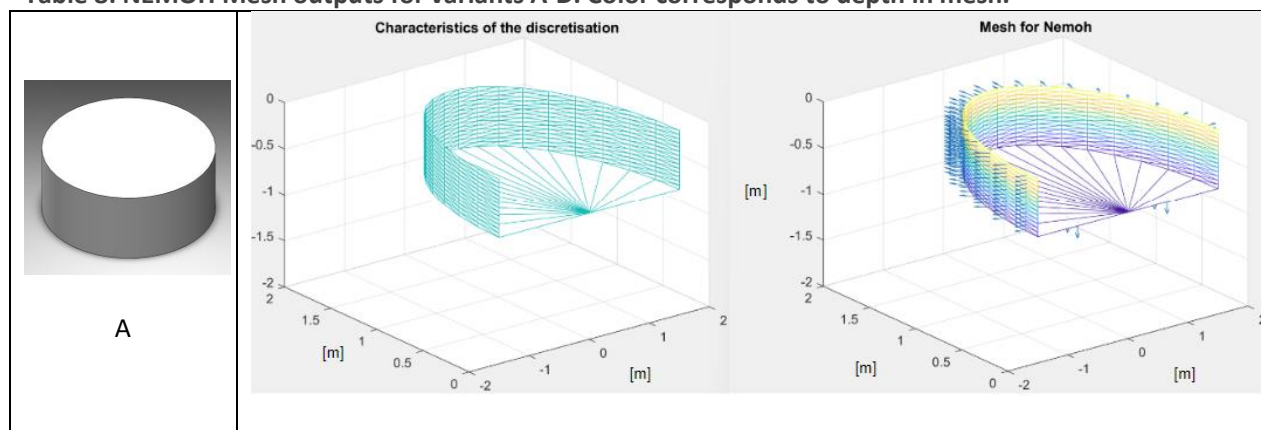
**NEMOH also generates two figures, a figure showing the characteristics of discretization (**

**Table 8, middle), and a figure showing the mesh with normal vectors for each discretization (**

**Table 8, right). The full rendering for the hull shape is shown in**

Table 8 on the left, along with its variant label (A-D). These full renderings were generated by Thomas Klodenski [44]. Because of the axisymmetric properties, and disregarding what happens above the waterline for simplicity, NEMOH only requires modeling a quarter of the hull geometry to calculate the outputs it needs, where the top of the NEMOH mesh figures is where the waterline sits on the hull.

**Table 8: NEMOH Mesh outputs for variants A-D. Color corresponds to depth in mesh.**



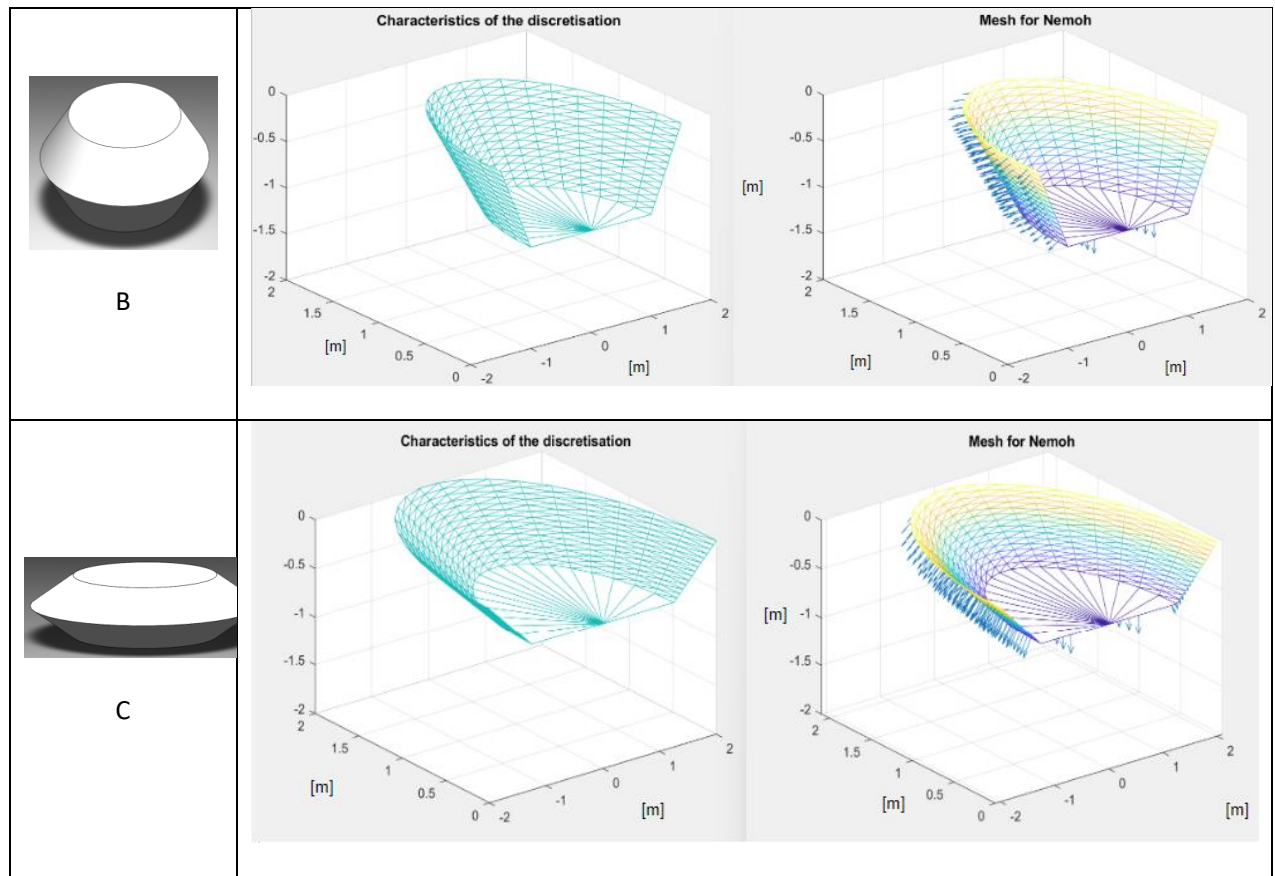
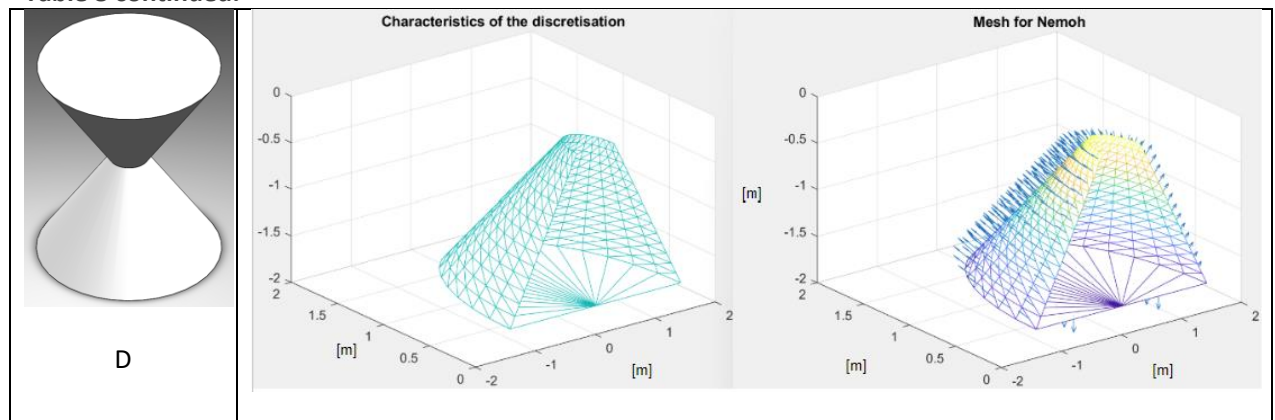


Table 8 continued.



NEMOH and other potential flow models allow for complex hull geometries to be modeled as a single point in water with its own unique set of hydrostatic and hydrodynamic quantities so that it can be tested and run as close as possible to the actual device. Certain limitations arise from using NEMOH. In certain wave energy applications, the linear nature of potential flow models may be compromised [45]. This raises the question of how effectively these devices can still be simulated using conventional linear tools. Moreover, standard commercial tools often do not inherently incorporate power take-off (PTO) mechanisms and control strategies, although they can be incorporated through user-defined functions. Consequently, this has prompted the emergence of specialized wave energy tools that rely on linearized potential flow theory to cater specifically to these requirements [45]. Using the outputs of the potential flow model in conjunction with these specialized tools (WEC-Sim being one) can help to accurately model WECs.

#### 4.2.4 NEMOH to WAMIT

**For the frequency domain model to use the NEMOH output files, they are converted to WAMIT**

**formatted files. A code created by Dr. Richard Kimball (refer to APPENDICES APPENDIX)** runs NEMOH and creates WAMIT style file outputs from NEMOH outputs. An added mass and radiation damping coefficient file is made into a WAMIT.1 file, shown in Figure 21, which includes the period at which values are calculated (with the 0 and infinite periods removed), the row and column number of the matrix at where the calculated values are placed in their respective matrix (corresponding to Figure 18, left, where the subsequent values represent “(row)’s effect on (column)”), and the added mass and damping coefficients.

Period at which values are calculated	Row of Matrix	Column of Matrix	Added Mass Coefficients	Damping Coefficients
1.256637E+02	1	1	1.910688E+00	0.000000E+00
1.256637E+02	1	2	0.000000E+00	0.000000E+00
1.256637E+02	1	3	0.000000E+00	0.000000E+00
1.256637E+02	1	4	0.000000E+00	0.000000E+00
1.256637E+02	1	5	0.000000E+00	0.000000E+00
1.256637E+02	1	6	0.000000E+00	0.000000E+00
1.256637E+02	2	1	0.000000E+00	0.000000E+00
1.256637E+02	2	2	1.910690E+00	0.000000E+00
1.256637E+02	2	3	0.000000E+00	0.000000E+00
1.256637E+02	2	4	0.000000E+00	0.000000E+00
1.256637E+02	2	5	0.000000E+00	0.000000E+00
1.256637E+02	2	6	0.000000E+00	0.000000E+00
1.256637E+02	3	1	0.000000E+00	0.000000E+00
1.256637E+02	3	2	0.000000E+00	0.000000E+00
1.256637E+02	3	3	7.731306E+00	0.000000E+00
1.256637E+02	3	4	0.000000E+00	0.000000E+00

Figure 21: ABwamit file annotated to show the meanings of the rows and columns.

The excitation forces output is made into a WAMIT.3 file, shown in Figure 22, which includes the periods at which the values are calculated, the direction of the incident wave exciting the body, the row of the matrix (or corresponding direction from Figure 18), the magnitude, angle, real part, and imaginary part of the excitation force calculated. The last two columns (columns 6 and 7) are used in the frequency domain code in section 4.3 .

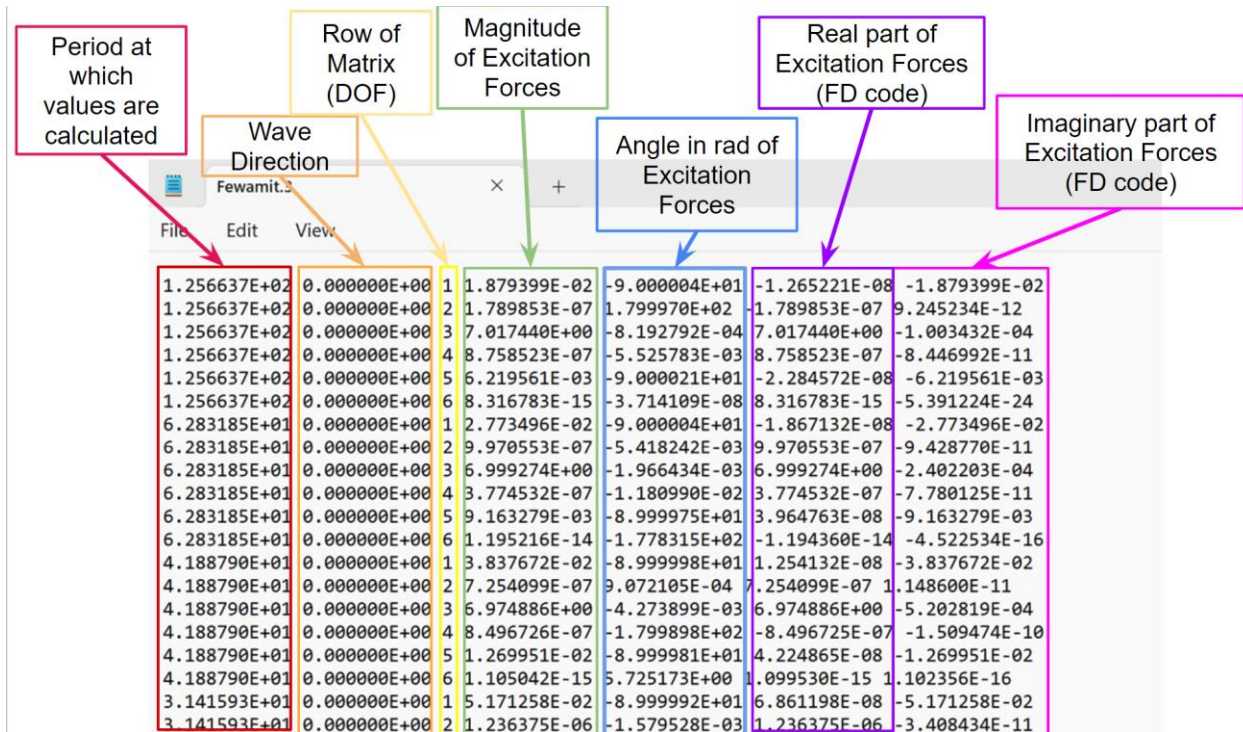


Figure 22: Fewamit file annotated to show the meanings of the rows and columns.

The hydrostatics outputs are placed in a HST WAMIT file, shown in Figure 23. This file includes the frequency at which the hydrostatic value is calculated at, the row and column of the hydrostatic matrix to which the value belongs, and the hydrostatic value in the last column. Columns 2 and 3 which represent the row and column of the hydrostatic matrix are read similarly to that of the ABwamit file in Figure 21, as “(row)’s effect on (column)”. The heave stiffness is pointed out in the figure, where row is equal to 3 (heave) and column is equal to 3 (heave).



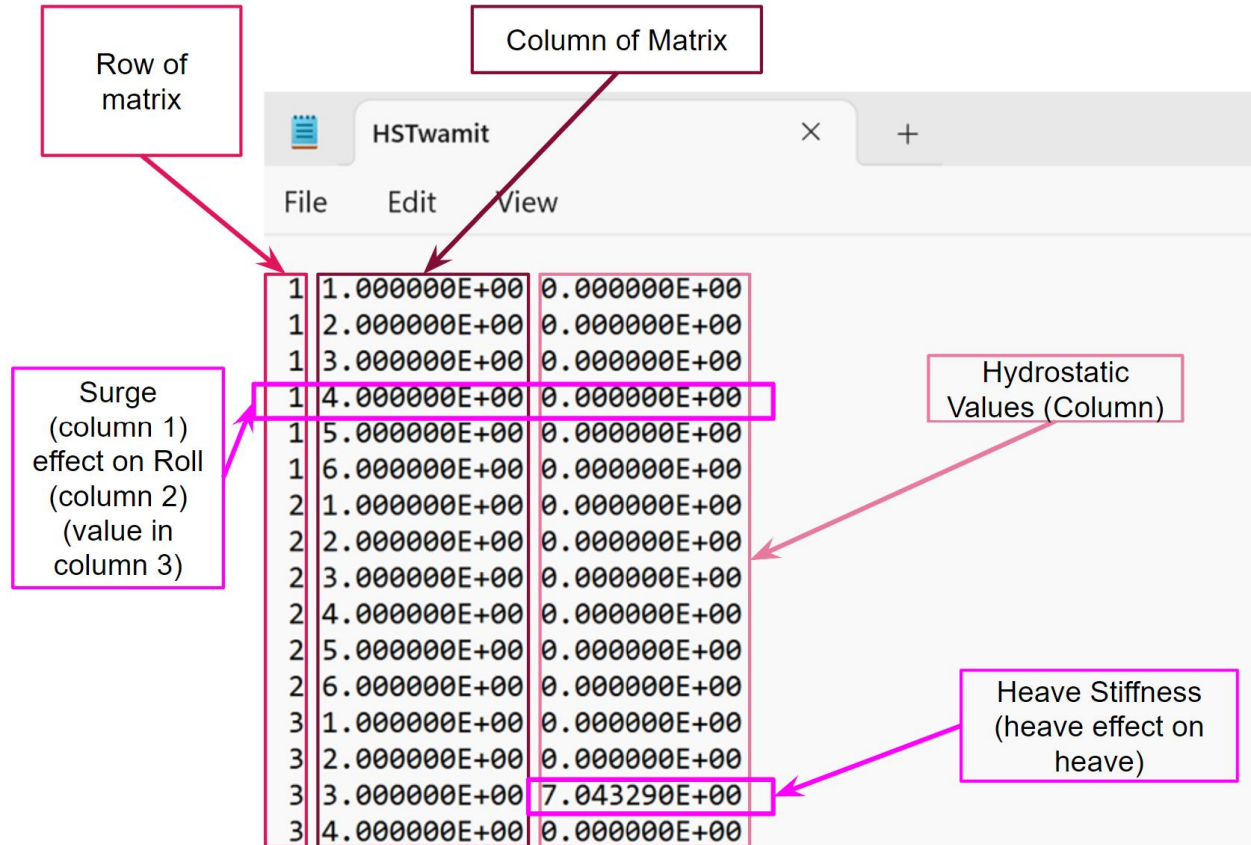


Figure 23: HSTwamit file annotated to show the meanings of the rows and columns.

Refer to APPENDIX B for the frequency domain code.

#### 4.3 Frequency Domain Model

The frequency domain model, developed by Dr. Andrew Goupee, uses a single degree of freedom equation of the heave motion to model the body. Using the hydrostatic and hydrodynamic outputs from NEMOH, the frequency domain model can calculate the response of the system due to different forcing frequencies [46] with the JONSWAP parameters of the most commonly occurring wave in CSOTS. The equation of motion of the system is shown in Equation 21 below as,

$$[M + M_{added}(\omega)]\ddot{x} + [B(\omega) + C_{PTO}]\dot{x} + [k_{hyd} + k_{mooring}]x = \bar{F}e^{i\omega t} \quad (21)$$

Where  $M$  is the mass of the system,  $M_{added}(\omega)$  is the added mass of the system (function of circular forcing frequency  $\omega$ ),  $B(\omega)$  is the radiation damping,  $C_{PTO}$  is the PTO damping,  $k_{hyd}$  is the hydrostatic stiffness,  $k_{mooring}$  is the mooring stiffness,  $\bar{F}e^{i\omega t}$  is the forcing function (force of the wave given by the JONSWAP), and,  $x$  and its derivatives are the position, velocity, and acceleration of the system. Assuming,

$$x(t) = \Re[Xe^{i\omega t}] = |X| \cos(\omega t + \varphi) \quad (22)$$

Where,  $X$  is amplitude of the response, and  $\varphi$  is the phase angle, given by:

$$\varphi = \tan^{-1} \left( \frac{(X)_{img}}{(X)_{real}} \right) \quad (23)$$

The phase angle is then substituted into Equation 22 and after canceling like terms we arrive at,

$$\left[ -\omega^2 [M + M_{added}(\omega)] + i\omega [B(\omega) + C_{PTO}] + [k_{hyd} + k_{mooring}] \right] X = \bar{F} \quad (24)$$

The PTO damping coefficient is calculated using the following equation:

$$C_{PTO} = 2\zeta \sqrt{(k_{hyd} + k_{mooring})(M + M_{added}(\omega_1))} \quad (25)$$

Where  $\zeta$  is the damping ratio:

$$\zeta = \frac{C_{PTO}}{C_{critical}} \quad (26)$$

Average Power can then be calculated as:

$$P_{avg} = \left| C_{PTO} \frac{i\omega X^2}{2} \right| \quad (27)$$

### **4.3.1 Frequency Domain Outputs**

Outputs of the frequency domain model are shown in

Table 9. Each two plots are shown in each row for each variant, one is the average power produced vs PTO damping coefficient given one input forcing frequency (the most commonly occurring full scale wave for the Castine site, shown in Figure 24), and the other plot is the average power produced as a function of PTO damping coefficient and forcing frequency. This frequency domain model output allows us to find the optimal value for the PTO damping coefficient and gives an idea of how much power on average the input geometry will produce at the most commonly occurring wave at the site. For the geometry of variant A (refer to

Table 8), the peak average power is 3.56 kW, and the optimal damping coefficient is calculated to be 50.76 kNs/m.

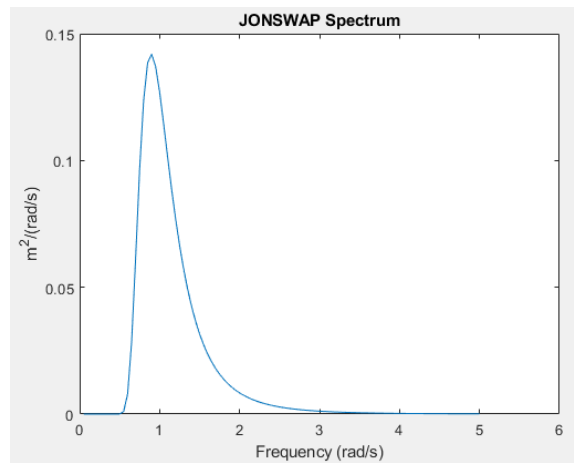


Figure 24: JONSWAP input to dynamic models of  $H_s = 1.2\text{m}$  and  $T_p = 7.0\text{s}$ .

**Table 9: Frequency domain outputs, average power vs PTO damping ratio on the left, and average power vs PTO damping ratio vs forcing frequency on the right for all variants (A-D)**

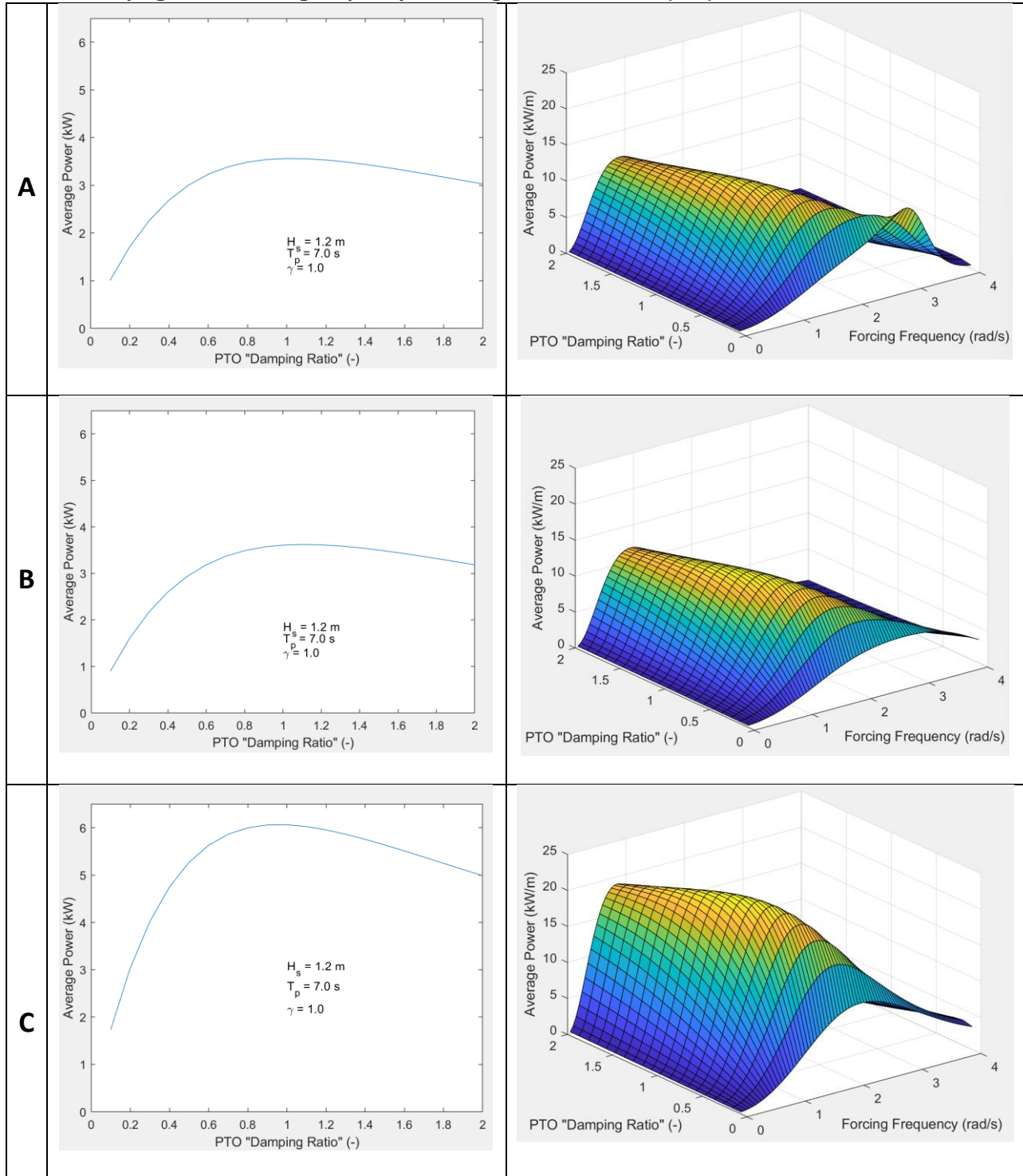
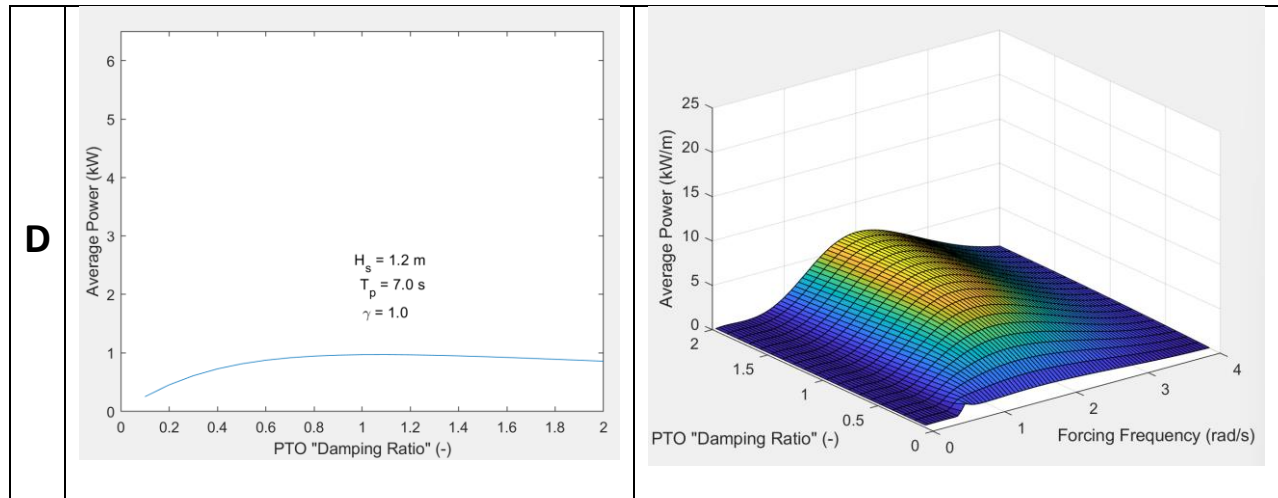


Table 9 continued.



The following Table 10 showcases the differences in waterplane area between the variants and their outputs and the peak average power and optimal damping coefficient outputs from the frequency domain model. There is a positive correlation between the waterplane area and the peak average power and damping coefficients from the model. This is to be expected, as the WEC is being modeled as a buoy that moves only in heave, so the force generated is proportional to the waterplane area of the device.

**Table 10: Variants and their waterplane areas, peak average power expected from the frequency domain model, and optimal damping coefficients.**

Variant	Waterplane Area (m <sup>2</sup> )	Peak Average Power (kW)	Damping Coefficient (kNs/m)
A	7.065	3.56	50.76
B	7.065	3.6246	53.89
C	12.56	6.089	102.79
D	0.28	0.96	11.59

Using the weightings for each wave case discovered in CHAPTER 2, this model could be run for each wave case in the environment and the average power output for each wave in the environment and the average power output for each wave case can be multiplied by its respective weighting and summed to amass the average power output generated over a whole year of device use.

#### 4.4 Time Domain Model

With the hydrostatic and hydrodynamic coefficients calculated, and the optimal PTO damping value found, the WEC can then be modeled in the time domain using WEC-Sim. WEC-Sim is an open-source code for simulating wave energy converters [47]. The internal WEC-Sim flow chart is shown in Figure 25.

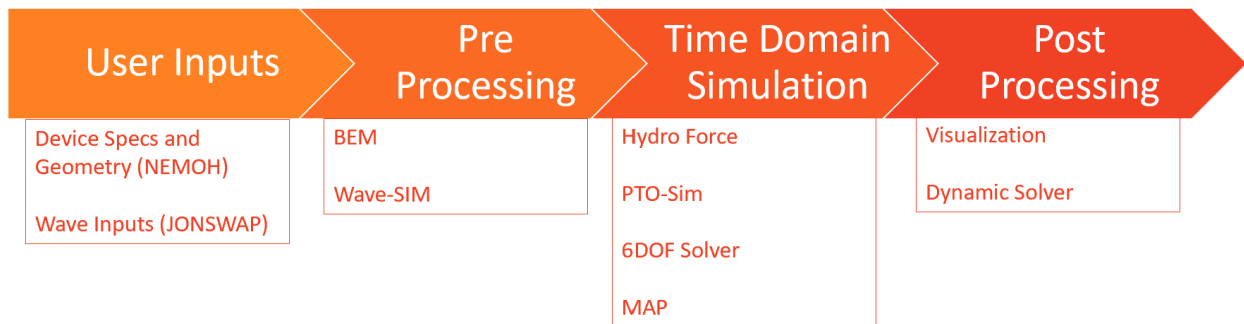


**Figure 25: Flow Chart Representation of WEC-Sim Inputs and Outputs from Potential Flow Model Geometry Definition Input to Output.**

Figure 26 shows the WEC-Sim time series output. The average power was computed to be 1.754. The damping coefficient used for this simulation was 20,000 Ns/m, which is below the optimal value found by the frequency domain model. This output from WEC-Sim was generated prior to the use of the frequency domain model. The outputs of WEC-Sim with the correct inputs for all of the variants is a good route for future work.

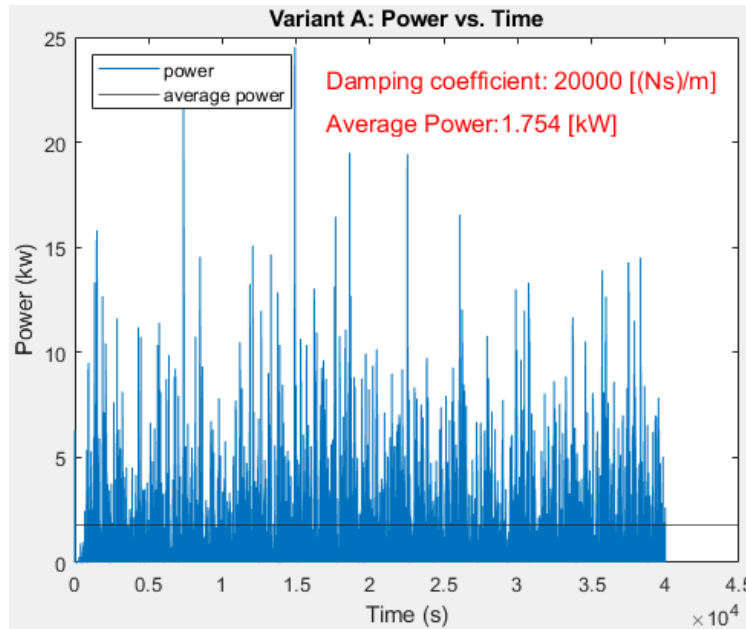


Figure 26: Time domain time series output.

#### 4.5 Discussion of Modeling Discussion

This chapter discusses the use of dynamic system models to capture the behavior of WECs in wave environments. Two types of dynamic models are described, a simplified frequency domain model and a time domain model. These models rely on force coefficients derived from a potential flow model, such as hydrostatic and hydrodynamic coefficients. This allows for the dynamic models to represent complex WEC hull geometries as a single point in the water with its own unique hydrostatic and hydrodynamic qualities.

The frequency domain model calculates power over a range of possible damping coefficients, which allows for the researcher to identify possible energy outputs of a given geometry, and to identify the optimal damping ratio and damping coefficient of the PTO by finding the value that creates the most energy in a



desired wave environment. The time domain model takes the optimal PTO damping value as an input and provides a time-series representation of power production, and an average can be calculated. The results of these two models can be used for experimental validation, and to make sure the models converge.

Throughout this chapter, the workflow and underlying methodology of each model are explained, and how they can be used with one another to model the devices. This chapter emphasizes the use of a WEC modeling workflow using tools that already exist rather than developing new ones. The models used in this chapter are open source and widely available, but there are advantages and disadvantages to each of them. Table 11 expands on each model’s strengths and weaknesses.

**Table 11: Potential Flow, Frequency Domain, and Time Domain Model Advantages and Disadvantages.**

<b>Model Type</b>	<b>Advantages</b>	<b>Disadvantages</b>
<b>Potential Flow Model – NEMOH</b>	Open source. Robust. Can be run from MATLAB. Gives mesh visuals.	Has known trouble with irregular frequencies and discontinuity. Written in Fortran
<b>Frequency Domain Model</b>	Simple, one degree of freedom model. Can easily be modified to model more degrees of freedom.	Does not account for nonlinear viscous effects and overestimates energy production, dependent on the potential flow model. Only models one degree of freedom. Restricted to linear problems; approximate in waves with small amplitudes relative to their wavelengths and less accurate otherwise.
<b>Time Domain Model – WEC-Sim</b>	Can be run from MATLAB. Models nonlinear PTO properties and control. Uses many potential flow model inputs, including NEMOH. Creates animations and visuals. Open source. Robust.	Requires MATLAB add-ons. Reportedly has trouble with NEMOH file inputs. Must include accurate PTO information for accurate results.

The models in this chapter were used because of their usability and advantages. The frequency domain and time domain models are both dynamic models that output average expected power based on the JONSWAP shown in Figure 24.

The two dynamic model outputs had different average power expectations for all the models. The frequency domain model gave consistently higher average power outputs for all the models than the WEC-Sim model. Figure 27 shows the outputs of both the time domain output (right) and the frequency domain output (left), with the average power vs damping shown in each. The frequency domain model outputs higher values of average power, but the two models behave similarly. A damping ratio of 1 is equal to around  $5.E+04$  Nm/s of damping.

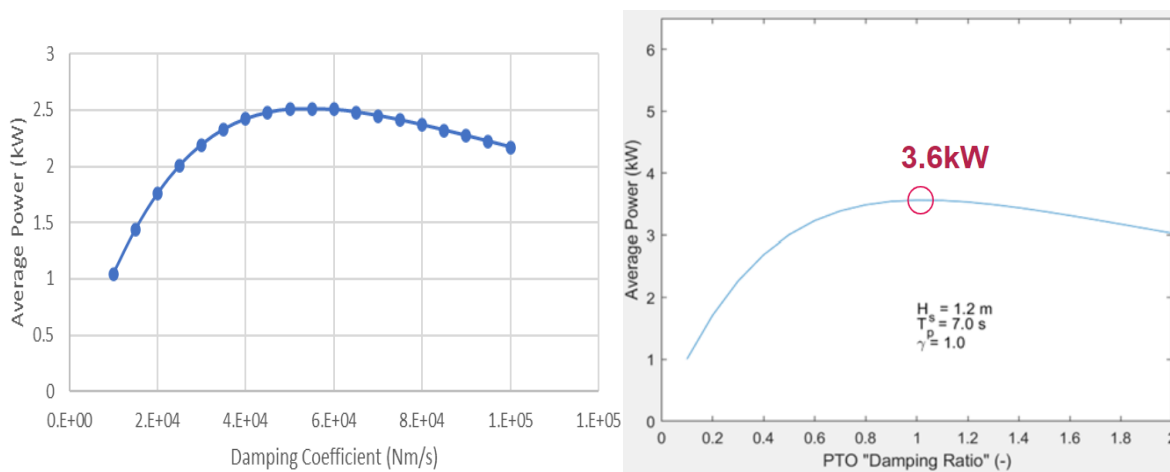


**Figure 27: Power output for the dynamic models: WEC-Sim time domain output is shown on the right and the frequency domain output is shown on the left.**

The frequency domain model shows higher average power output because the model is very stripped down and is limited to linear problems. The frequency domain model does not account for nonlinear viscous effects, wave breaking, wave steepness, and is only applicable for small amplitude waves. Additionally, the frequency domain model does not facilitate PTO control strategies other than constant PTO coefficients [43]. The WEC-Sim model can include PTO affects and calculations that are described in its user manual [41] that the frequency domain model does not account for. Future modeling using the frequency domain model will continue to serve as the preliminary tool to inform parameter ranges of interest. The time

domain model can then be used to produce higher-fidelity results that facilitate the goal of scale model testing. This sequential modeling workflow can produce results efficiently for researchers to use in their studies. In the future, it is suggested to note the effects of nonlinear hydrostatic stiffnesses from basin testing to compare to how well the linear potential flow model predicted the nonlinear behaviors. For use in the SAM metric described in CHAPTER 3, the average power can be multiplied by the hours in a year and multiplied by average profit for kWhr of energy produced by the device to get a gross profit from the device per year.

## CHAPTER 5

### Test Plan Development for WECs

#### 5.1 Overview

The final step in the design\build\test loop is to test the design variants, so that desirable variants can be chosen to make a hybrid to be designed, built, and tested in the basin during the original testing timeline. A test plan is developed to establish a protocol by which the designs can be tested to ensure that the runs are all uniform, the campaign objectives are achieved, and instrumentation is properly set up. The objectives of the test campaign are to design and construct the scale model test components that use additive manufacturing methods, instrument the WEC, design an optimal variant to be built during the test campaigns and test it for comparison, assess the results using the performance metrics. This chapter will be organized according to the following layout for the test plan, with brief details of each section. This layout is as follows:

1. Testing facility description.
2. Froude scaling laws.
3. Device description and properties.
4. Data acquisition.
5. Test matrix and testing conditions.

#### 5.2 Testing Facility Description

The University of Maine's Advanced Structures and Composites Center (ASCC), shown in Figure 28, is an ISO 17025 accredited interdisciplinary research and testing center that was established by the National Science Foundation in 1996 that includes a wind and wave (W2) testing center (Figure 29) for all offshore applications. The W2 is a 9m x 30m x 5m, 16-paddle basin equipped with a wind tunnel that can simulate various scale-model tests. The test plan [48] details the wave basins capabilities and limits.



Figure 28: Drone view of the Advanced Structures and Composites Center testing facility. The wave basin is in the back of the facility.

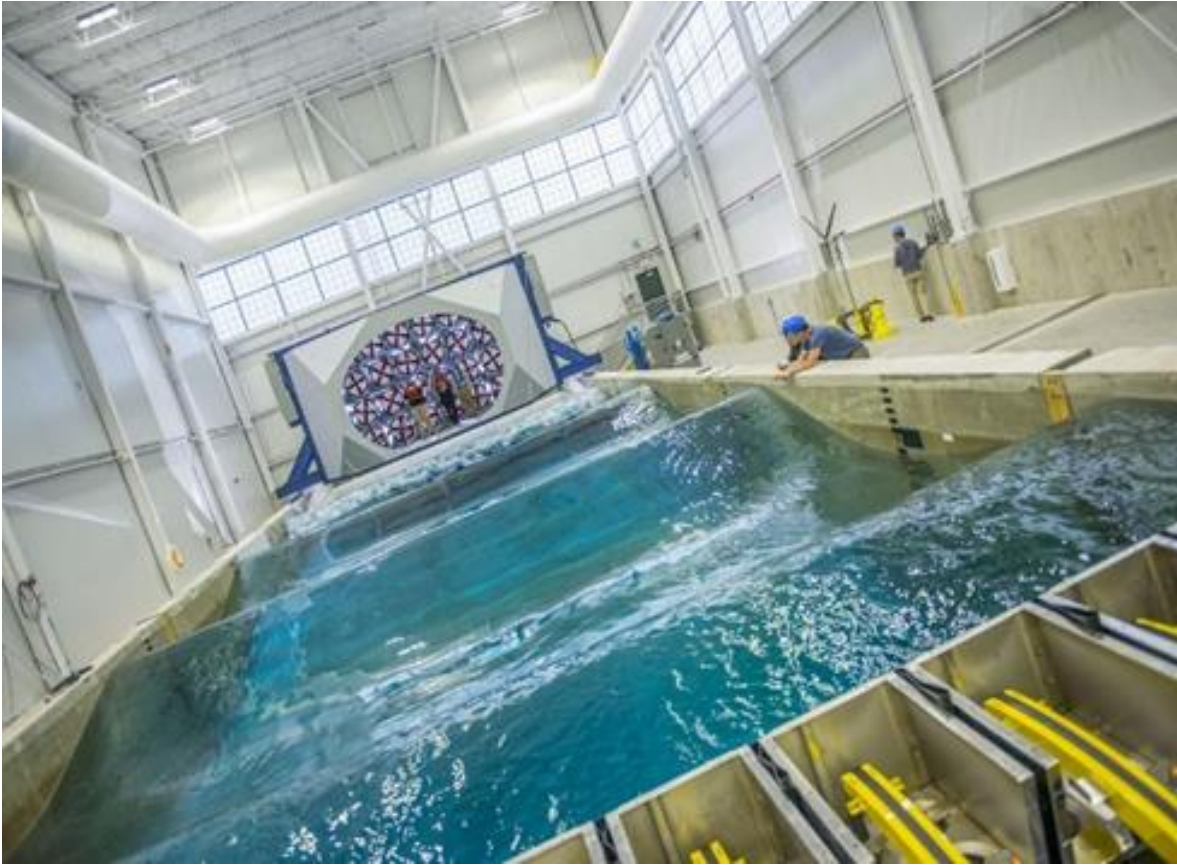


**Figure 29: The wave basin at the Advanced Structures and Composites Center used to run the tests described in this chapter. The bottom of the picture shows the wave makers, and at the top of the basin a wind wall can be seen.**

The basin's wave paddles are run using the Edinburgh Designs Njord Wave Synthesis software that allows for researchers to specify waves and calibrate the basin for each wave run. This software can also be used to identify what waves are not possible in the wave basin, which allows engineers and researchers to redesign their test campaigns if need be.

### **5.3 Froude Scaling Laws**

The test campaigns in the wave basin use Froude scaling as its convention for quantities of interest. The data is recorded at model-scale and presented at full scale using the scaling factors shown in Table 12. The scale of the model is defined by  $\lambda$  as the ratio between the full-scale and model-scale lengths, and  $\varphi = 1.025$ . Full scale values are found by multiplying the model data by the scale factors in Table 12. The scale

factor of 1:7 was chosen for this test campaign due to the geometric scaling relationship found in CHAPTER 2.

The far-left column of Table 12 shows the actual scale values after inserting the scale ratio and  $\varphi$  quantities.

**Table 12: Froude scaling factors.**

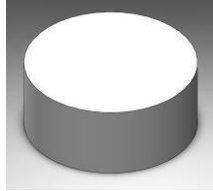
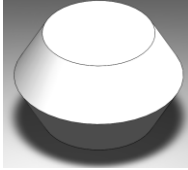
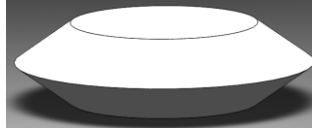

Quantity	Scale Factor	Value
Length/Position	$\lambda$	7
Velocity	$\lambda^{0.5}$	2.65
Acceleration	1	1
Angle	1	1
Angular Velocity	$\lambda^{-0.5}$	0.38
Angular Acceleration	$\lambda^{-1}$	0.14
Time	$\lambda^{0.5}$	2.65
Frequency	$\lambda^{-0.5}$	0.38
Mass	$\lambda^3 \varphi$	351.58
Mass Moment of Inertia	$\lambda^5 \varphi$	17227.18
Force	$\lambda^3 \varphi$	351.58
Moment/Torque	$\lambda^4 \varphi$	2461.03

#### 5.4 Device Description

The device is a point absorber, as modeled in CHAPTER 4, whose PTO cable is attached directly below the hull to the seabed. The hull was identified to be the component to be optimized during the test campaign, and the four design variations from CHAPTER 4 are to be tested in the campaign. The hull variants will use a shared mooring line and control system which is anchored to the basin floor and lead to a wall-mounted PTO as shown in Figure 17. The PTO is modeled as a winch on the tank side.

The test plan includes descriptions of all the hull variants proposed for testing, shown in Table 13. Each variant is to be 3D-printed in the ASCC. Results from testing these variants will be used to inform the design of a hybrid, optimized model to maximize energy production according to the metrics in CHAPTER 3. Due to the nature of the objectives of the testing, the final optimized model is to be designed, built, and tested during the testing of the other variants.

**Table 13: WEC design variants for test plan.**

	<p><b>Variant: A</b></p> <p>Height: 18.2 cm</p> <p>Radius: 21.4 cm</p> <p>Volume: 0.026 m<sup>3</sup></p>		<p><b>Variant: B</b></p> <p>Height: 25.8 cm</p> <p>Radius: 14.8 cm</p> <p>Waterline Radius: 21.4 cm</p> <p>Volume: 0.026 m<sup>3</sup></p>
	<p><b>Variant: C</b></p> <p>Height: 15.2 cm</p> <p>Radius: 17.9 cm</p> <p>Waterline Radius: 28.6 cm</p> <p>Volume: 0.026 m<sup>3</sup></p>		<p><b>Variant: D</b></p> <p>Height: 48.3 cm</p> <p>Radius: 20.3 cm</p> <p>Waterline Radius: 4.3 cm</p> <p>Volume: 0.026 m<sup>3</sup></p>

The PTO is designed and built by a WEC company and is modeled as a winch at the side of the basin. The test plan outlines the specifics of how the PTO is connected to the WEC hull. The PTO will be actively controlled and will manage the WEC mooring forces to adjust the winch according to the desired damping forces.

Waves will be calibrated using wave calibration probes. Calibration probes are resistive wave probes that are used for tuning the basin's wavemaker to the desired wave environment described in the test plan. The resistance probes are calibrated using an integrated five-point depth range that is included in the Edinburgh Designs wave maker VI. These resistance probes are removed after calibration, at which point the



model is deployed. Figure 30 shows the schematic for the layout of the calibration probes (designated “C”), and the reference probes (designated “R”). The reference probes are in place to continue to monitor the wave environment and adjust if need be and provide reference measurements at non-model locations. More information and model numbers of probes are provided in the test plan.

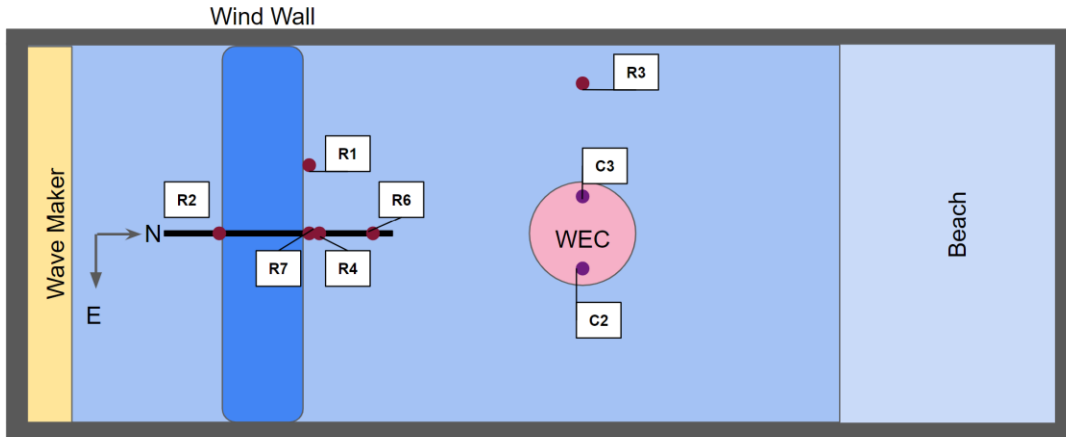


Figure 30: A top view of the basin with the WEC in it. Points designated "R" refer to reference probe locations, where points designated "C" are calibration probe locations.

### 5.5 Data Acquisition

The basin is equipped with Qualisys motion tracking, Oqus cameras, and Miquis cameras to track body movement and take data. The above water cameras and origin (AQ) and the underwater cameras and origin (UQ) are shown in the schematic in Figure 31. Qualisys cameras, such as the Oqus cameras, track the motion of bodies with reflective adhesive markers that are placed on the hull. Origins are also designated with this adhesive to act as a “zero” point for calibration. The Miquis cameras are used just for video recordings of tests. The information from the motion tracking creates 4 files for each run, a QTM motion tracking file, a MATLAB file, and two video files for above water and below water tracking.

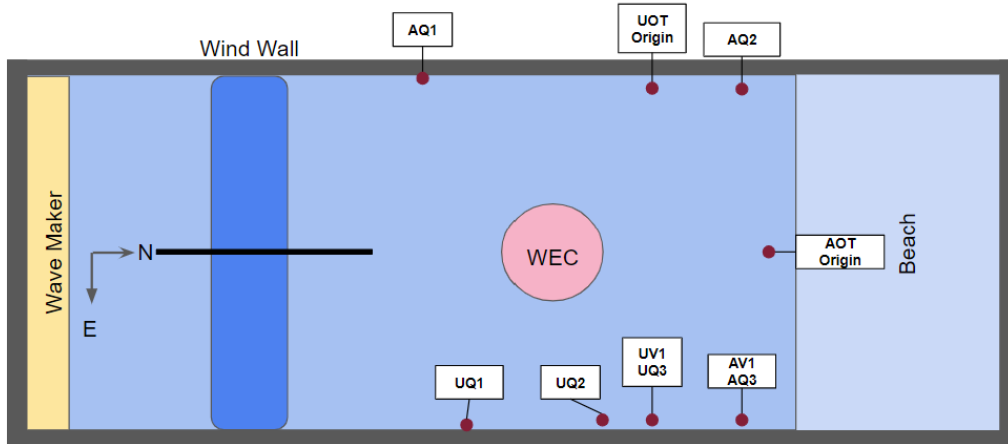


Figure 31: A top view of the basin with the WEC in it. Points designated "AQ" refer to above-water Qualisys cameras, and points labeled "UQ" refer to underwater Qualisys cameras.

Load cells are used to measure tension in the mooring line, and an encoder will be used to obtain PTO velocity tracking in this instrumentation strategy.

### 5.6 Test Matrix and Test Conditions

The test runs are chosen from the 1:7 scale heatmap obtained in CHAPTER 2 to best represent the environment. This includes the most commonly occurring wave at 9.79% occurrence in the yellow box in Table 14. The waves in yellow were proposed by the device manufacturer.

Table 14: 1:7 scale heat map indicating which waves are to be used for testing in the test plan.

		%									100%	
		0.34	3.45	14.56	25.51	27.64	18.49	7.63	2.10	0.28		
Hs (m)	0.29				0.01		0.03	0.1	0.06	0.01	0.18	%
	0.27			0.01	0.31	1.64	2.63	1.45	0.41	0.12	6.57	
	0.24			0.26	2.11	4.12	3.57	1.39	0.64	0.05	12.15	
	0.22		0.11	1.38	3.64	4.76	3.75	1.66	0.43	0.03	15.76	
	0.19		0.4	2.57	5.93	6.74	3.8	1.74	0.29	0.03	21.51	
	0.17	0.16	1.01	5.77	9.79	8.17	4	1.25	0.23	0.04	30.42	
	0.14	0.18	1.93	4.57	3.74	2.22	0.71	0.04	0.03		13.41	
	0.12										0.00	
		2.25	2.31	2.49	2.66	2.84	3.02	3.20	3.37	3.55		
		Tp (s)										

Each variant will be tested in all of the chosen wave environments, 2 heave free decay test runs (to confirm natural heave periods and calculate viscous damping coefficients), and 1 PTO characterization run (for PTO tuning). The test plan includes time estimates for each wave run, as the basin requires 20 minutes of settling time between wave runs. Several tank side tests are also described in the test plan to ensure that the physical properties of the designs are recorded including a geometry verification and a center of gravity verification. In the tank, each design variant is placed in the basin and the ballast is distributed to verify that the model sits at a level trim before any test runs in the water are done.

Once testing is complete and data is acquired, the data can be processed through the metrics created in CHAPTER 3, and results can be compared to the model results captured in CHAPTER 4. As basin testing is currently ongoing at the time of completion of this thesis, more time is to be dedicated to completing basin testing and verifying convergence with the models and metrics.

## CHAPTER 6

### Conclusions

The successful development and optimization of wave energy converters (WECs) are pivotal to the pursuit of sustainable and renewable energy sources. In this thesis, the essential components for advancing the understanding of WEC testing and optimization through wave site characterization of scaled ocean test sites, performance metric development, modeling, and basin testing were addressed. The outcomes of this study have considerable significance for the industry of wave energy development, helping to further the understanding of accurate and reliable testing protocols which will ultimately accelerate the adoption of wave energy as a viable source of energy. Figure 32 shows the entire process of the efforts of this thesis starting with the wave environments determination through the final test plan of WEC systems. Step 1 (wave site collection and data analysis) corresponds to chapter 1. Step 2 (metric development) represents chapter 3. Step 3 (modeling) shows the outcomes of chapter 4, and Step 4 (test plan development) represents chapter 5.

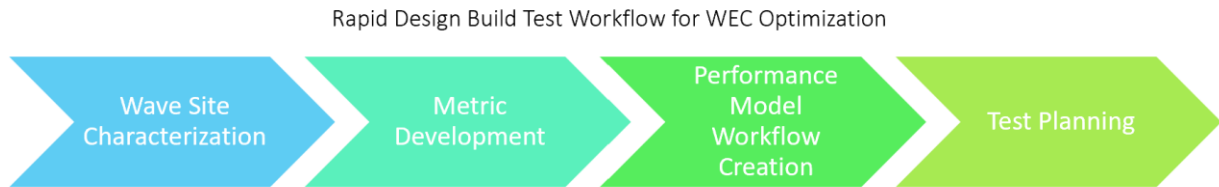


**Figure 32: Rapid design\build\test workflow for WEC optimization.**

Through wave site characterization, valuable insights were gained into wave climate parameters and how to find the scale ratio for testing. The comprehensive analysis of significant wave heights, peak periods, direction, and JONSWAP content provided an accurate representation of the wave conditions at CSOTS that the WECs are most likely to encounter in deployment. By incorporating this information into the modeling and testing processes, researchers and engineers can conduct test campaigns that accurately simulate the obstacles and advantages posed by different wave conditions.

Developing metrics for performance evaluation was another key aspect of this thesis. By establishing normalized and objective metrics, fair and accurate comparisons between different WEC design iterations were made possible, helping to identify the strengths and weaknesses of each design. These metrics produce a systematic and dependable pathway to evaluate WEC design iteration performance, streamlining the design process, and promoting advances in their technology.

The formulation of a WEC modeling workflow for the rapid design\build\test loop will help the variants to be tested according to the test plan and will help to calibrate the models to evaluate different variants based on testing to determine an optimum design which is to be constructed during the basin test and then evaluated to complete the optimization process. These models helped to inform expectations when testing models and help to understand the similarities and differences in device modeling versus experimental outcomes. These models could then also be used to calculate expected yearly energy production values of different WEC design iterations using the heat map of the wave site's wave climate probabilities and directions.

The implication of a test plan was then the final step in this thesis. The combination of the wave environment curated from chapter 2 and the metrics developed from chapter 3, guided by the information found in chapter 4 lead to a well-informed development of a test plan that could be used for further testing. This testing will eventually lead to the decision of the most optimal design shape which will lead to a full-scale model to be built and deployed. The process described in this these could be used to any wave energy converter development and may help streamline the processes that are used today.

## **6.1 Future Work**

Future work suggestions include measuring yearly variations in wave climate conditions at multiple different test sites of interest, creating metrics that help to evaluate lifespan of devices using fatigue information from materials in salt water, using WEC-Sim to evaluate yearly average energy productions using the heat maps of wave environments, and applying all the metrics to basin testing and scaled ocean test site

testing outputs. Exploring the dynamic interactions between multiple WECs within a test site, such as extreme weather events and other environmental factors like salinity and impact on wildlife are all promising areas for future investigations.

This study is limited by the usability and availability of potential flow and time domain models, as well as robust frequency domain models that can accurately model WEC PTOs. Additionally, this study is limited by the basin testing information that is available at the time of publishing, where the energy generating WEC models are yet to be tested in the basin and therefore the energy generation metrics cannot be applied with accurate data.

In conclusion, this thesis provides a comprehensive exploration of wave site characterization, WEC modeling, metric development, and basin testing workflows. The findings and methodologies presented in this study have the potential to shape future research, industry practices, and policy frameworks in the domain of energy. As we strive for a more sustainable future, the knowledge gained in this study will play a crucial role in harnessing the energy potential of ocean waves and reducing our reliance on nonrenewable energy.

## BIBLIOGRAPHY

- [1] V. Masson-Delmotte, P. Zhia, A. Pirani, S. L. Connors and C. Pean, "Climate Change 2021 The physical Science Basis Summary for Policymakers," *Intergovernmental Panel on Climate Change (ipcc)*, 2021.
- [2] M. Melikoglu, "Current status and future of ocean energy sources: A global review," *Ocean Engineering*, vol. 148, pp. 563-573, 2018.
- [3] A. B. Gill, "'Offshore Renewable Energy: Ecological Implications of Generating Electricity in the Coastal Zone.'" *Journal of Applied Ecology*, vol. 42, no. 4, pp. 605-615, 2005.
- [4] L. Dickson, L. Ross and R. Kimball, "Wave Environment Characterization for Scaled Ocean Test Sites," in *Oceans22*, Hampton Beach, VA, 2022.
- [5] H. Martin, "Development of a Scale Model Wind Turbine for Testing of Offshore Floating Wind Turbine Systems," *M.S. Thesis, University of Maine, Orono, ME*, 2011.
- [6] The European Marine Energy Center LTD (EMEC), "Pathway to Commercialisation," [Online]. Available: [www.emec.org.uk](http://www.emec.org.uk). [Accessed 16 May 2023].
- [7] Y. Zhu, L. Jia, C. Duan, X. Sun and W. Guo, "Status of testing field for ocean energy generation," *Journal of Modern Power Systems and Clean Energy*, vol. 5, pp. 160-168, 2017.
- [8] B. Cahill and T. Lewis, "Wave energy resource characterization and the evaluation of potential Wave Farm sites," *OCEANS'11 MTS/IEEE KONA*, pp. 1-10, 2011.
- [9] A. Cornett, "A Global Wave Energy Resource Assessment," in *International Offshore and Polar Engineering*, Vancouver, Canada, 2008.
- [10] B. Cahill and A. W. Lewis, "Wave Energy Resource Characterization of the Atlantic Marine Energy Test Site," in *European Wave and Tidal Energy Conference*, Southampton, UK, 2011.
- [11] P. Yuan, S. Wang, H. Shi, P. Guo and Z. Dong, "Overview and proposal for development of ocean energy test sites in China," *2012 Oceans, Yeosu*, 2012.
- [12] C. Allen, "Metocean and Wind Site Conditions for Monhegan Island, Maine," University of Maine's Advanced Structures and Composites Center, 2020.
- [13] R. Atan, G. Jamie, M. Harnett, P. Agostinho and S. Nash, "Assessment of wave characteristics and resource variability at a 1/4-scale wave energy test site in Galway Bay using waverider and high frequency radar (CODAR) data," *Ocean Engineering*, vol. 117, pp. 272-291, 2016.
- [14] G. Iglesias and R. Carballo, "Wave energy resource in the Estaca de Bares area (Spain)," *Renewable Energy*, vol. 35, no. 7, pp. 1574-1584, 2010.

- [15] A. M. Viselli, A. J. Goupee, H. J. Dagher and C. K. Allen, "Design and model confirmation of the intermediate scale VoltturnUS floating wind turbine subjected to its extreme design conditions offshore Maine," *Wind Energy*, vol. 19, pp. 1161-1177, 2015.
- [16] Fisherman.org, "Penobscot Bay Nautical Chart," [Online]. Available: <https://usa.fisherman.org/depth-map/penobscot-bay-maine/>. [Accessed 2022].
- [17] D. Dhvani, "A Review of various statistical methods for outlier detection," *International Journal of Computer Science & Engineering Technology (IJCSET)*.
- [18] University of Maine, "Wave Energy Prize Tests," Orono, 2016.
- [19] A. Karimpour, "Oceanlyz," github.com, 2022. [Online]. Available: <https://github.com/akarimp/Oceanlyz>. [Accessed 2021].
- [20] K. Hasselmann, T. Barnett, E. Bauws, H. Carlson and et.al, Measurements of Wind-Wave Growth and Swell Decay during the Joint North Sea Wave Project (JONSWAP), Hamburg: Deutsches Hydrographisches Institut, 1973.
- [21] National Weather Service Weather Prediction Center, "Meteorological Conversations and Calculations: The Beaufort Wind Scale," [Online]. Available: <https://www.wpc.ncep.noaa.gov/html/beaufort.shtml>. [Accessed 31 August 2022].
- [22] H. Abdi, "The Method of Least Squares," *Encyclopedia of Measurement and Statistics*, 2007.
- [23] University of Maine Advanced Structures and Composites Center, "VoltturnUS Floating Concrete Hull Technology," [Online]. Available: <https://composites.umaine.edu/research/voltturnus/>. [Accessed 31 August 2022].
- [24] B. A. Groen, M. J. Wouters and C. P. Wilderom, "Employee participation, performance metrics, and job performance: A survey study based on self-determination theory," *Management Accounting Research*, vol. 36, pp. 51-66, 2017.
- [25] M. Fujita, Y. Domae, A. Noda, G. Garcia Ricardez, T. Nagatani and A. Zeng, "What are the important technologies for bin picking? Technology analysis of robots in competitions based on a set of performance metrics," *Advanced Robotics*, vol. 1, no. 34, p. July, 2019.
- [26] A. M. Petersen and O. Penner, "Renormalizing individual performance metrics for cultural heritage management of sports records," *Chaos, Solitons, & Fractals*, vol. 136, 2020.
- [27] S. W. West, J. Clubb, L. Torres-Ronda, D. Howells, E. Leng, D. D. Vescovi, S. Carmody, M. Posthumus, T. Dalen-Lorentsen and J. Windt, "More than a Metric: How Training Load is Used in Elite Sport for Athlete Management," *International Journal of Sports Medicine*, vol. 42, no. 4, pp. 300-306, 2021.
- [28] OpenEI, "Marine Energy Performance Metrics," PRIME, 2022. [Online]. Available: <https://openei.org/wiki/PRIMRE/Telesto/Metrics>. [Accessed May 2023].



- [29] H. Li, C. Qi, Y. Tao, H. Liu, W. Da-Wei, F. Li, Q.-H. Yang and H.-M. Cheng, "Quantifying the Volumetric Performance Metrics of Supercapacitors," *Advanced Energy Materials*, 17 April 2019. [Online]. Available: <https://onlinelibrary.wiley.com/doi/abs/10.1002/aenm.201900079>. [Accessed 10 May 2023].
- [30] C. Elrod, S. Murray and S. Bande, "A Review of Performance Metrics for Supply Chain Management," Taylor & Francis Online, 20 April 2015. [Online]. Available: <https://www.tandfonline.com/doi/abs/10.1080/10429247.2013.11431981>. [Accessed 10 May 2023].
- [31] S. Mirjalili and A. Lewis, "Novel performance metrics for robust multi-objective optimization algorithms," *Swarm and Evolutionary Computation*, vol. 21, pp. 1-23, 2015.
- [32] N. Riquelme, C. Von Lüken and B. Baran, "Performance metrics in multi-objective optimization," *Latin American Computing Conference (CLEI)*, pp. 1-11, 2015.
- [33] B. Niu, H. Hwangbo, L. Zeng and Y. Ding, "Evaluation of alternative power production efficiency metrics for offshore wind turbines and farms," *Renewable Energy*, vol. 128, no. A, pp. 81-90, 2018.
- [34] A. Babarit, J. Hals, M. Muliawan, A. Kurniawan, M. T. and J. Krokstad, "Numerical benchmarking study of a selection of wave energy converters," *Renewable Energy*, vol. 41, pp. 44-63, 2012.
- [35] G. Giannini, P. Rosa-Santos, V. Ramos and F. Taveira-Pinto, "Wave energy converters design combining hydrodynamic performance and structural assessment," *Energy*, vol. 249, 2022.
- [36] A. Garcia-Teruel and D. Forehand, "A review of geometry optimisation of wave energy converters," *Renewable and Sustainable Energy Reviews*, vol. 139, 2021.
- [37] OpenEI, "Levelized Cost of Energy," PRIMRE, [Online]. Available: [https://openei.org/wiki/PRIMRE/Telesto/Metrics/Levelized\\_Cost\\_of\\_Energy](https://openei.org/wiki/PRIMRE/Telesto/Metrics/Levelized_Cost_of_Energy). [Accessed 2023].
- [38] F. R. Driscoll, J. W. Weber, D. S. Jenne, R. W. Thresher, L. J. Fingersh, D. Bull, A. Dallman, B. Gunawan, K. Ruehl, D. Newborn, M. Quintero, A. LaBonte, D. Karwat and B. Scott, "Methodology to Calculate the ACE and HPQ Metrics Used in the Wave Energy Prize," National Renewable Energy Lab (NREL), Golden, CO (U.S.), 2018.
- [39] National Renewable Energy Laboratory (NREL), "System Advisor Model (SAM)," 2020. [Online]. Available: <https://sam.nrel.gov/>. [Accessed 2023].
- [40] R. Kurnia and G. Ducrozet, "NEMOH v3.0 User Manual," 2022.
- [41] "WECsim - Theory," [Online]. Available: <https://wec-sim.github.io/WEC-Sim/theory.html>. [Accessed 6 7 2023].
- [42] WAMIT, Inc., "WAMIT USER MANUAL V. 7.4," Massachusetts Institute of Technology, Boston, MA, 2020.
- [43] M. Alves, "Frequency-Domain Models," in *Numerical Modelling of Wave Energy Converters*, Lisbon, Portugal, Elsevier, 2016, pp. 11-30.

- [44] T. Klodenski, *Full Renderings of Hull Variants*, Orono, 2023.
- [45] F. Wendt, K. Nielsen and e. al, "Ocean Energy Systems Wave Energy Modelling Task: Modelling Verification and Validation of Wave Energy Converters," *Journal of Marine Science and Engineering*, vol. 7, no. 11, 2019.
- [46] S. S. Rao, *Mechanical Vibrations*, Pearson, 2011.
- [47] D. K. Ogden, Y.-H. Yu, A. Keester, D. Forbush, J. Leon and N. Tom, "Review of WEC-Sim Development and Applications," *DOE Pages*, pp. 293-303, 2022.
- [48] N. Faessler, R. Kimball, L. Ross and L. Dickson, "Calwave Test Plan," University of Maine's Advanced Structures and Composites Center, Orono, Maine, 2023.
- [49] P. Lenee-Bluhm, R. Paasch and H. T. Ozkan-Haller, "Characterizing the energy resource of the US Pacific Northwest," *Renewable Energy*, vol. 36, pp. 2106-2119, 2011.
- [50] D. Pereira, "Wind Rose," MATLAB Central File File Exchange, 2023. [Online]. Available: <https://www.mathworks.com/matlabcentral/fileexchange/47248-wind-rose>.

## APPENDICIES

### APPENDIX A

#### NEMOH to WAMIT File Conversion Code

---

```
Rm=1.5 %m
Rk=1.5 %m Rb
Keel=-0.637 %m must be negative as it is below waterline
rho=1024
g=9.81
invrhog=1/rho/g
n=16
%r=[ R*ones(1,(n-1)) 0]
zb=0:(Keel/(n-2)):Keel
z=[ zb Keel]
r=[ (Rk+(Keel+abs(zb))/Keel*(Rm-Rk)) 0]
[Mass, Inertia, KH, XB, YB, ZB]=axiMeshMEE489(r, z, n);
KH
Mass
ZB
%Write KH hydrostatic stiffness matrix in wamit.hst format Wamit
fileID = fopen('HSTwamit.hst','w');
    for i = 1:6 %i is the ith row force in the FEmatrix
        for j=1:6
            KH_out = [i j KH(i,j)*invrhog];
            fprintf(fileID, '%i %1.6E %1.6E\r\n', KH_out);
        end
    end
end

fclose(fileID)
```

---

```
% %runNEMOH for spar

% %Setup by WHR 11/23/2020
%inputs for NEMOH run function from NEMOH.cal file
%w = .001 is for inf period
%w = 100 is for inf freq
rho=1025
g=9.81
irhog=1/(rho*g)
w=[0.025 10 0.05:.05:4]; %period~1 sec to 100sec freq=0.01hz to 1hz
% first two are zero to infinite.
dir=0;
depth=200;
[A,B,Fe]=Nemoh(w, dir, depth);

%write added mass A and Damping B text files Wamit.1 format
```

```

T=2*pi./w
fileID = fopen('ABwamit.1','w');
n=1;
for p = 1:length(T) %p cycles through periods
    for i = 1:6;%i is the ith row in the added mass matrix
        for j = 1:6;%the jth column in the added mass matrix
            if A(i,j,p)<100;
                A(i,j,p)=0;
            end;
            if B(i,j,p)<100;
                B(i,j,p)=0;
            end;
            if p==1;
                T(p)=-1;
                A_out = [T(p) i j A(i,j,p)/rho];
                fprintf(fileID,'%1.6E %i %i %1.6E\r\n',A_out);
            else;
                if p==2;
                    T(p)=0;
                    A_out = [T(p) i j A(i,j,p)/rho];
                    fprintf(fileID,'%1.6E %i %i %1.6E\r\n',A_out);
                else;
                    %A_out(n,:) = [w(p) i j A(i,j,p)/rho B(i,j,p)/rho/w(p)];
%writes in parsible format
                    A_out = [T(p) i j A(i,j,p)/rho B(i,j,p)/rho/w(p)];
                    fprintf(fileID,'%1.6E %i %i %1.6E %1.6E\r\n',A_out);
                end;
            end;
            n=n+1;
        end;
    end;
end;
fclose(fileID);

%Write Fe external forces in wamit.3 format Wamit
fileID = fopen('Fewamit.3','w');
for p = 3:length(T); %p cycles through periods
    for i = 1:6 %i is the ith row force in the FEmatrix
        Fe_out = [T(p) dir i abs(Fe(p,i))*irhog,...
            angle(Fe(p,i))*180/pi,real(Fe(p,i))*irhog,imag(Fe(p,i))*irhog];
        fprintf(fileID,'%1.6E %1.6E %i %1.6E %1.6E %1.6E %1.6E\r\n',Fe_out);
    end;
end;
fclose(fileID);

```

---

## APPENDIX B

```
%Rich's Wave Energy Device Optimizer - A Really Simple One
%A. Goupee
%Last modified: 4/18/2023

%Set system properties
m_p = 2333; %Physical mass (kg)
k_m = 0; %Vertical mooring stiffness (N/m)
V_o = 4.32; %Displaced volume (m^3 - not used)

%Set water and planet properties
rho = 1025; %Water density (kg/m^3)
g = 9.8065; %Acceleration due to gravity (m/s^2)

%Solve for pretension
T_p = V_o*rho*g-m_p*g; %Vertical pretension (N - not used)

%Read in data files
K_n = load('HSTwamit.hst'); %Normalized hydrostatic stiffnesses
AB_n = load('ABwamit.1'); %Normalized added mass and radiation damping,
%infinite period and frequency entries removed
F_n = load('Fewamit.3'); %Normalized wave excitation forces

%Extract information needed for solution of harmonic motion
k_h = K_n(15,3)*rho*g; %Heave hydrostatic stiffness (N/m)

N = size(AB_n)/36; %Number of periods
for i = 1:N; %Loop through periods
    w(i) = 2*pi/AB_n(36*(i-1)+15,1); %Frequency (rad/s)
    A(i) = AB_n(36*(i-1)+15,4)*rho; %Heave added mass (kg)
    B(i) = AB_n(36*(i-1)+15,5)*rho*w(i); %Radiation damping (Ns/m)
    F(i) = (F_n(6*(i-1)+3,6)+1i*F_n(6*(i-1)+3,7))*rho*g; %Wave excitation
    % force per unit amplitude wave - complex (N)
end;

%Set wave parameters
Hs = 1.19; %Signicant wave height (m)
Tp = 7.04; %Peak period (s)
gamma = 1.0; %Peak shape parameter (-)
f = w/(2*pi); %Frequencies (Hz)
[Sj] = JONSWAP(f,Hs,Tp,gamma); %Obtain JONSWAP spectrum
Sjw = Sj/(2*pi); %Spectrum in m^2/(rad/s)

%Plot added mass, radiation damping ans wave excitation force for a check
% figure(1)
% clf
% hold on
% box on
% plot(w,A,w,B,w,abs(F))
% xlabel('Frequency (rad/s)')
% legend('A_3_3 (kg)', 'B_3_3 (Ns/m)', 'X_3 (N/m)')
```

```

%Set damper values to consider
zeta = [0.1:0.1:2]; %Damping ratios for PTO
c_pto = zeta*2*sqrt((k_h+k_m)*(m_p+A(1))); %PTO damping values (Ns/m)

for j = 1:length(c_pto); %Loop through pto damping values

    c_pto_j = c_pto(j); %Set damping value

    for i = 1:N; %Loop through frequencies

        %Solve for complex amplitude/phase
        Z = -(w(i)^2)*(m_p+A(i))+1i*w(i)*(B(i)+c_pto_j)+(k_h+k_m);
        X = inv(Z)*F(i);

        X_h(j,i) = abs(X); %Amplitude (m/m)
        p_h(j,i) = atan2(imag(X),real(X)); %Phase (rad)

        %Determine vertical velocity
        X_dot = 1i*w(i)*X;

        X_dot_h(j,i) = abs(X_dot); %Amplitude ((m/s)/m)
        p_dot_h(j,i) = atan2(imag(X_dot),real(X_dot)); %Phase (rad)

        %Determine power production amplitude
        Powt = c_pto_j*(X_dot_h(j,i)^2)/2;
        Pow(j,i) = abs(Powt); %Average (W/m)

    end;

end;

%Estimate average power
dw = w(2)-w(1);
for j = 1:length(c_pto); %Loop through pto damping values

    Pavg(j) = sqrt(sum((Pow(j,:)).^2).*Sjw'*dw));

end;

% %Plot heave RAO magnitude
% figure(2)
% surf(w,zeta,X_h)
% xlabel('Forcing Frequency (rad/s)')
% ylabel('PTO "Damping Ratio" (-)')
% zlabel('Heave RAO Magnitude (m/m)')

% %Plot heave velocity RAO magnitude
% figure(3)
% surf(w,zeta,X_dot_h)
% xlabel('Forcing Frequency (rad/s)')
% ylabel('PTO "Damping Ratio" (-)')
% zlabel('Heave Velocity RAO Magnitude ((m/s)/m)')

%Plot power 'RAO magnitude'

```

```

figure(4)
axis equal
surf(w,c_pto,Pow/1000)
xlabel('Forcing Frequency (rad/s)')
ylabel('PTO Damping Coefficient (Ns/m)')
zlabel('Average Power (kW/m)')
xlim([0 4])

% %Plot wave spectrum
% figure(5)
% clf
% hold on
% box on
% plot(w,Sjw);
% xlabel('Frequency (rad/s)')
% ylabel('m^2/(rad/s)')
% title('JONSWAP Spectrum')

%Plot average power as a function of PTO damping setting
figure(6)
clf
hold on
box on
plot(c_pto,Pavg/1000);
xlabel('PTO Damping Coefficient (Ns/m)')
ylabel('Average Power (kW)')
text(0.5*max(zeta),0.5*max(Pavg/1000),['H_s = ' num2str(Hs,'%1f') ' m'])
text(0.5*max(zeta),0.43*max(Pavg/1000),['T_p = ' num2str(Tp,'%1f') ' s'])
text(0.5*max(zeta),0.36*max(Pavg/1000),['\gamma = '
num2str(gamma,'%1f')])

```

## **BIOGRAPHY OF AUTHOR**

Lauren Dickson was born in Biddeford, Maine on September 10, 1998. She was raised in Arundel, Maine and graduated from Thornton Academy in 2016. She attended the University of Maine in Orono and graduated in 2021 with a Bachelor's of Science Degree in Mechanical Engineering. She returned to the University of Maine for graduate school immediately upon receiving her Bachelor's. After receiving her degree, Lauren will begin her career as an engineer and a renewable energy advocate, with the hope of pursuing a doctorate. Lauren is a candidate for the Master of Science degree in Mechanical Engineering with a concentration in Offshore Renewable Energy from the University of Maine in August 2023.